Faculty of Science

Mesoscale precipitation systems in the Tibetan Plateau region as represented by global reanalysis, regional downscaling and satellite data between 2001 - 2016

Benjamin Holmberg

Degree of Master of Science (120 credits)
with a major in Earth Sciences
60 hec

Department of Earth Sciences
University of Gothenburg
2022 B1200

UNIVERSITY OF GOTHENBURG

UNIVERSITY OF GOTHENBURG
Department of Earth Sciences
Geovetarcentrum/Earth Science Centre

Mesoscale precipitation systems in the Tibetan Plateau region as represented by global reanalysis, regional downscaling and satellite data between 2001 - 2016

Benjamin Holmberg

ISSN 1400-3821

B1200
Master of Science (120 credits) thesis
Göteborg 2022

Mailing address
Geovetarcentrum
S 405 30 Göteborg

Address
Geovetarcentrum
Guldhedsgatan 5A

Telephone
031-786 19 56

Geovetarcentrum
Göteborg University
S-405 30 Göteborg
SWEDEN

Abstract.

The Tibetan Plateau (TP) is one of the world's most important water towers. Convective precipitation systems play an important role by providing freshwater for the highly densely populated downstream regions, but they can also cause hazardous floods. Most of the convective processes occur at mesoscale where a spatiotemporal knowledge gap still exists in climate model simulations in mountainous regions. This report aims to bring new information to this knowledge gap by analyzing how convective precipitation systems are represented in two Regional Climate Model (RCM) simulations: the Weather Research and Forecasting simulation from the University of Gothenburg (WRF_GU) and the High Asia Refined analysis version 2 (HAR). The datasets differ in the techniques used to resolve mesoscale convective processes and in how they incorporate large-scale circulations. We have also conducted analyses using a coarser global reanalysis dataset (ERA5) and satellite observations (GPM) for comparison. We have defined a convective precipitation system as Mesoscale Precipitation Systems (MPSs) to include all convection on a scale larger than local. These have later been tracked using an object-based approach, which enables a more detailed temporal analysis of their characteristics and evolvement as we can follow their every timestep during a lifecycle.

Our results showed that the two RCM simulations detected more MPSs over the TP compared to ERA5 and GPM. In the larger domain, HAR detected most while WRF_GU the least. We could also see that MPSs contributed with a significant amount of precipitation, even in drier regions. MPSs tended to peak post-midnight in the larger domain while during the afternoon over the TP. Due to its coarse resolution, early convection was not detected in ERA5. This was evident in its delayed timing of MPS convection and low number of detected MPSs over the TP. These findings suggest an added value of using a higher spatial resolution when analyzing convection in mountainous regions. Furthermore, our results implicate that an RCM simulation using CP and re-initialization caused excessive convection while a non-CP RCM simulation using spectral nudging resulted in the opposite. By tracking MPSs at every timestep of their lifecycle, it was also found that longer lived systems were more prone to produce intense precipitation with distinct peaks and lows during a day compared to smaller ones. We believe the findings of our research could be valuable in further analyses of mesoscale convection using RCM simulations of different spatial and temporal resolution, with and without CP. We also believe that more research such as this can help fill the spatiotemporal knowledge gap in modelling mesoscale convective processes. In the end, this could aid in accurately modelling convective systems in water scarce regions dependent on them for freshwater and affected by them in terms of hazardous floods.

Keywords: Tibetan Plateau, monsoon, westerlies, mesoscale, convection, precipitation, climate modelling, global reanalysis, regional downscaling, spatial resolution, re-initialization, spectral nudging, convective parameterization

Contents

1 Introduction

1.1 Tibetan Plateau

1.1.1 Hydrological importance

The Tibetan Plateau (TP) has an average altitude of 4000 m and includes some of the world's largest mountain ranges e.g Karakorum (western TP) and the Himalayas (southern TP) (Yao et al., 2011). The high altitude of the TP has resulted in a large ice storage which has led to the term "The Third Pole" (Qiu, 2008). The TP is thereby a large source of freshwater where many important rivers (e.g. the Indus, Ganges and Yangtze) originate from, rivers that bring freshwater resources to a large part of the Asian population. The downstream regions are also extremely densely populated and have a large irrigation demand, which makes the TP one of the world's most important water towers (Immerzeel et al., 2019; Immerzeel et al., 2010). The many rivers and complex topography combined, however, makes this area highly vulnerable to floods if struck by heavy and instant precipitation, which has been shown to often originate from convective precipitation systems (Houze Jr, 2004; Kotal et al., 2014; Kuo et al., 1986; Rasmussen & Houze, 2012).

1.1.2 Impact of large-scale circulations and precipitation

The subtropical westerly jet plays an important role in the formation and location of precipitation in the TP region. During winter, the westerly jet brings moist air towards the TP where it is orographically lifted, triggering convection and precipitation in the western parts of the TP region (Curio & Scherer, 2016). Simultaneously, the TP splits the westerly jet, causing subsidence over northern India and although temperatures increase during spring, this subsidence still suppress convection south-southeast of the TP (Sato & Kimura, 2007). When the westerly jet migrates northwards in early summer, however, subsidence weakens and enables intense convection and precipitation. This shift also defines the onset of the Indian monsoon, which lasts between June – August, and is the period of most intense rainfall of the region (Sato & Kimura, 2007; Wang et al., 2018).

Temperature differences between the TP and its surroundings during winter and summer also play an important role for the region's precipitation pattern as it enables a surface divergence (winter) and convergence (summer) wind flow over the TP (Yanai & Wu, 2006). In summer, i.e. during the Indian monsoon, this results in moist air being drawn from the Bay of Bengal (BoB) towards the TP where it is blocked by the Himalayan mountain range, triggering convection and precipitation south of it. As a result, precipitation is intense in the northern parts of the Indian subcontinent, with highest precipitation southeast of the TP, decreasing gradually towards the west along the Himalayan mountain range (Maussion et al., 2014).

1.2 Convective precipitation

1.2.1 Formation and scale

As suggested by Doswell III (1987), convection is often initiated by processes at the mesoscale which can later form to organized systems. Convective precipitation can therefore come in many forms and be involved in various precipitation systems on different spatiotemporal scales, from sub-hourly small-scale tornadoes to extratropical cyclones lasting for days (Orlanski, 1975). In the midlatitudes convective precipitation is a common feature while in the tropics, it constitutes most of the precipitation (Houze Jr, 1981; Ye et al., 2017). Stratiform precipitation can, however, occur as some convective precipitation systems mature (Houze Jr, 1981).

Atmospheric moisture and temperature gradient, together with a lifting mechanism, are all needed for deep convection to be triggered. In order to develop into larger systems, wind shear is also necessary (Schumacher & Rasmussen, 2020). Some processes at the mesoscale which can trigger convection are mountain-valley circulations, orographic forcing, land-sea breeze and solar heating causing unstable stratification (Houze, 2012; Orlanski, 1975; Qin et al., 2009). These processes occur on a relatively small spatiotemporal scale and are, therefore, problematic in model simulations (Ye et al., 2017). Furthermore, although individual storms of smaller scale bring precipitation, it is often in concentrated short-lasting showers. Most precipitation rather originates from organized systems at larger spatial scale, e.g. a squall line, even though they are less numerous (Houze Jr, 1981).

1.2.2 Mesoscale Convective Systems

One certain type of organized convective precipitation system is the Mesoscale Convective System (MCS). Of convective storms MCSs are the largest, they are common in the tropics and midlatitudes and have a pronounced seasonal cycle with most MCSs occurring between May and August (Houze Jr, 2004; Schumacher & Rasmussen, 2020). MCSs are often accountable for hazardous weather and can bring intense precipitation resulting in floods (Houze Jr, 2004; Schumacher & Rasmussen, 2020), e.g. east of the Rocky Mountains where MCSs were responsible for 65% of the extreme precipitation events during a three year period (Schumacher & Johnson, 2005). Due to global warming, MCSs have also been found to increase in both lifetime and precipitation intensity (Great Plains) and in frequency (Western African Sahel) (Schumacher & Rasmussen, 2020).

1.2.3 Convection in the TP region

Tibetan Plateau Vortices (TPVs) are precipitation systems at mesoscale unique for the TP. They occur mainly between May – August, are initiated over the northwestern TP and can bring up to 70% of total precipitation in the TP central region (Curio et al., 2019; Feng et al., 2014). TPVs usually have a west-east movement and if they move out of the plateau, the resulting precipitation can be catastrophic (Curio et al., 2019; Kuo et al., 1986).

Previous studies have shown that precipitation originating from MCSs, and other convective precipitation systems at mesoscale such as TPVs can be large contributors to the TP region's total precipitation. The numbers, however, varies a lot and are quite distinct depending on which region, or system, you focus on (Curio et al., 2019; Feng et al., 2021; Kukulies et al., 2021; Yaodong et al., 2008). Besides the contribution from organized systems, it has also been shown that precipitation originating from all convective processes constitutes a large proportion of the annual total over the Himalayan mountain range, while it can be close to nothing over parts of the TP (Maussion et al., 2014).

Additionally, during the past fifty years, temperatures over the TP have increased (Qin et al., 2009). This has caused changes in the hydrological cycle of the TP and enabled more favorable conditions for convection (Qiu, 2008; Yao et al., 2022). Over the Eurasian continent as a whole e.g., convective precipitation has been shown to increase during the past three decades of the 20th century as a consequence of increased temperatures, especially in daily precipitation extremes (Ye et al., 2017). MCSs and other convective precipitation systems in the TP region are therefore important both in a regional climate context and for the water cycle of this region, but also in understanding the possible risks associated with extreme weather events (Kotal et al., 2014; Rasmussen & Houze, 2012; Schumacher & Rasmussen, 2020).

1.2.4 Tracking precipitation systems

The object-based approach identifies precipitation areas that are independent from adjacent regions. (Davis et al., 2006; Ebert & McBride, 2000). This enables a tracking of individual precipitation systems where characteristics such as lifetime, size and diurnal occurrence can be identified and used for analysis (Davis et al., 2006a; Davis et al., 2006b). It further enables us to study the individual systems and their characteristics at different stages of their lifecycles, rather than the overall convection in an area during a certain period of time. Additionally, since the spatiotemporal scales of mesoscale processes varies, looking at each timestep of a convective precipitation system could also allow for a deepened intercomparison between the various datasets of different spatial resolution.

1.3 Modelling convective precipitation

1.3.1 Convective parameterization

By using climate data obtained from satellite observations and climate model simulation runs, previous studies have detected and analyzed convective precipitation systems in the TP region (Hu et al., 2017; Romatschke & Houze, 2011; Sato et al., 2008; Sugimoto & Ueno, 2012; Yaodong et al., 2008). The spatial resolution and techniques used in a model simulation play an important role in analyzing mesoscale convection (Sato et al., 2008; Weisman et al., 1997). For example, while data with coarser spatial resolution demands less storage and could be useful in global large-scale system analyses, it might be too coarse to identify convective processes, at mesoscale (Feser et al., 2011). They will therefore need to depend on a technique called convective parameterization (CP), which is implemented in the model simulations to represent the physical processes of

convection (Rummukainen, 2010). Previous research has shown that at a horizontal grid spacing of 4 km, spatial resolution is high enough for convection to be resolved explicitly instead, so called convection-permitting models (CPM). As a result, convection dynamics are better represented leading to an increased performance to detect convection and estimate precipitation, when compared to coarser CP model runs (Clark et al., 2016; Finney et al., 2019; Prein et al., 2013, 2021; Scaff et al., 2020). Finer resolution model runs, however, increases the computational power demand (Feser et al., 2011; Giorgi & Mearns, 1999; Prein et al., 2015). Additionally, there is a knowledge gap between convection-permitting and coarser resolution model runs (spatial resolution between 4 - 10 km), defined as the gray-zone of climate data modeling where convection is either parameterized or explicitly resolved (Prein et al., 2015). Although conducting model simulation runs with a spatial resolution within the gray-zone has been shown to cause errors when using CP (Finney et al., 2019; Kirshbaum, 2020; Ou et al., 2020; Pearson et al., 2014; Prein et al., 2015; Yu & Lee, 2010), it is not clear whether or not deep convection is sufficiently resolved when performing a model run within the gray-zone without CP (Ou et al., 2020; Yu & Lee, 2010). Exploring model simulation runs focusing on convection and precipitation in the gray-zone with and without CP is therefore complicated but also of great importance, since it could have a major impact on the final product.

1.3.2 Regional downscaling

A common approach to obtain information on a finer scale is to dynamically downscale data from either a General Circulation Model (GCM), or a global reanalysis dataset, to a smaller domain using a Regional Climate Model (RCM) (Feser et al., 2011; Giorgi & Mearns, 1999; Prein et al., 2015; Rummukainen, 2010). To still include large-scale circulations and enable their influence on the smaller chosen domain, the RCM will rely on boundary conditions from the data used for driving the model simulation (Giorgi & Mearns, 1999; Rummukainen, 2010). To avoid the RCM to drift away from the large-scale circulation conditions in continuous simulations over a long period of time, it can be re-initialized (updated) on a set interval by conditions from the driving data at the boundaries of the RCM domain. This technique is called re-initialization (Pan et al., 1999; Qian et al., 2003). Another approach is to use the spectral nudging technique where some chosen parameters in the model (e.g. wind components and moisture flux) are constantly nudged (pushed) to the conditions of the driving data. As a result, large-scale information is enabled to influence within the RCM domain as well, not just at its boundaries (Rummukainen, 2010; Spero et al., 2014; Von Storch et al., 2000; Waldron et al., 1996). Further, the higher spatial resolution used by the RCM will also resolve more detailed processes within its domain (Rummukainen, 2010), e.g. a better representation of topographical characteristics on a wider scale, enabling processes such as orographic drag and mountain-valley circulation (Feser et al., 2011; Lin et al., 2018). This, in turn, has been shown to result in a better representation of convection and precipitation in areas of complex terrain (Lin et al., 2018; Prein et al., 2013; Wagner et al., 2018; Zhao et al., 2021). Both spatial resolution and model simulation techniques are therefore important factors that should be carefully considered in convection and precipitation analyses when using climate model simulation data and in regional downscaling.

1.4 Aim

Since the late 1980s, convective processes at the mesoscale have been recognized as those most complicated to forecast (Doswell III, 1987). As for modern climate modelling, uncertainties still remain in how well mesoscale processes occurring on a sub-grid scale are resolved and how they interplay with large-scale circulations (Shepherd, 2014). Additionally, due to the lack of stationary observations and fairly recent increase of high-resolution climate modelling in the TP region, a spatiotemporal knowledge gap still exists in modelling convection and precipitation in this regions, as well as in other mountainous regions (Bao & Li, 2020; Yao et al., 2022). A deepened knowledge in how convective precipitation systems at the mesoscale are represented in datasets of different spatial resolution, and how different downscaling techniques couple large-scale circulations to a smaller domain, might help to fill this knowledge gap. The aim of this study is, therefore, to elucidate spatiotemporal characteristics of convective precipitation systems and how these are represented in various datasets. We have focused on the area around the TP, as this is a region highly involved and impacted by mesoscale convective dynamics. It is also a region vulnerable to climate change, as it modifies the TP's hydrological cycle (Immerzeel et al., 2019; Yao et al., 2022). We believe that this new information could be valuable for future studies focusing on convective dynamics at the mesoscale using RCM and CPM simulations. More specifically, this could be in the development process of RCM and CPM simulations and help the interpretation of future simulations of convective precipitation. It could also be helpful in other studies focusing on convective precipitation in a climate change context, e.g. in predicting future changes of the hydrological cycle in regions vulnerable to both floods and water scarcity (Bao & Li, 2020; Yao et al., 2022). To do so, we have focused on the following research questions:

- What are the main characteristics of mesoscale precipitation systems in the TP region between 2001 - 2016?
- How do these differ in the three model/reanalysis datasets that represent different spatial resolutions?
- Which of the two downscaling techniques result in the better representation of mesoscale precipitation systems compared to satellite observations?

This report will be structured as follows: a result section where analyses are divided into subsections based on their temporal or spatial nature, followed by a discussion of results where they are put into context to regional climatic patterns, spatial resolution, and model simulation techniques, then finally a section of concluding remarks.

2 Method

In this study, we will use output data from an objective tracking algorithm that detects large contiguous areas of precipitation in every timestep and links them over time (Heikenfeld et al., 2019). This tracking will be conducted using two dynamically downscaled RCM simulations with and without CP at a spatial resolution of 10 and 9 km respectively focusing on the TP region, known for its complex topography. Additional tracking using a global reanalysis dataset of coarser resolution and satellite observations for comparison will be performed as well. Results will be presented in a comparative study using the outputs from the climate model simulations and identify possible differences between and to the satellite observations. We have focused on the area between 26 - 44°N and 67 – 104°E defined as the extensive domain and over the TP only (TP domain) using the > 3000 m definition by Qin et al., (2009) (Fig. 1).

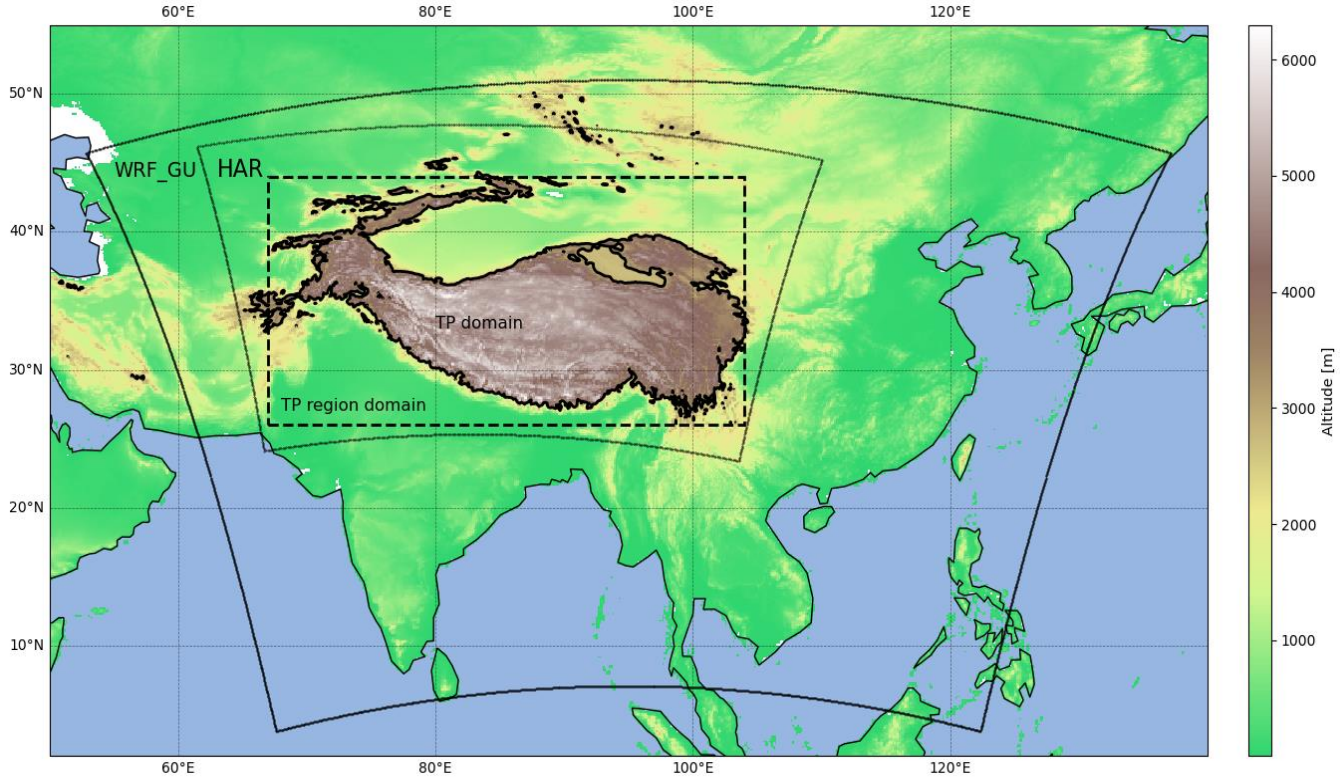

Figure 1. Elevation in the TP region including the extent of the two study areas used in this report: extensive domain and the TP defined as the area > 3000 m in altitude (TP domain), as well as the WRF_GU and HAR dataset extent.

2.1 Data

The two main datasets for analysis were the Weather Research and Forecasting downscaling product by Ou et al., (2020) from the Regional Climate Group at the University of Gothenburg (WRF_GU) and the High Asia Refined analysis version 2 (HAR)

product by Wang et al., (2021). Both datasets focus on the TP region and are dynamically downscaled regional climate model simulations driven with the European Centre for Medium-Range Weather Forecasts (ECMWF) ERA5 data set using the Weather Research and Forecasting model (WRF) (Ou et al., 2020; Wang et al., 2021). The WRF_GU product has a spatial resolution of 9 km, uses spectral nudging to constrain the large-scale circulations within the model domain and does not include CP (Ou et al., 2020). The HAR product has a spatial resolution of 10 km, it uses re-initialization to avoid drifting away too much from the large-scale circulations over time and CP enabled (Wang et al., 2021). Since both WRF_GU and HAR are driven by ERA5, this dataset will be used as a reference data. The ERA5 is a global reanalysis dataset (i.e. combined observation and forecast modeling) which uses re-initialization and CP with a spatial resolution of 31 km (Hersbach et al., 2020). Due to the scarcity of rain gauge stations in the over the TP, the Global Precipitation Measurement Mission IMERG Final Run (GPM) satellite product will be used as a comparative dataset. The GPM provides a global coverage of precipitation measurements obtained by satellites and it has a spatial resolution of 0.1° (approximately 10 km) (Hou et al., 2014). Each dataset has been subset to the area between 26 - 44°N and 67 – 104°E and to the years 2001 - 2016 to obtain joint spatial and temporal coverage.

2.2 Tracking Mesoscale Precipitation Systems

2.2.2 Definition and tracking

In this study, we have defined an organized convective precipitation system as Mesoscale Precipitation System (MPS). The thresholds used for our definition were chosen to exclude individual storm systems on a local scale but, also, to include other organized systems at mesoscale than e.g. MCSs. We therefore modified the definition for an MCS used in Feng et al. (2021) so that an MPS, by definition, has a shorter lifetime and minimum area threshold. This means that MCSs, as defined by Feng et al., (2021), are included but not explicitly tracked.

By using the Tracking and Object-Based Analysis of Clouds (tobac) algorithm, MPSs between 2001 – 2016 were identified over the TP and surroundings. Tobac was developed for identifying and tracking clouds and to be used in e.g. model intercomparison studies (Heikenfeld et al., 2019). The work flow in identifying an MPS can be seen in Fig. 2 (simplified and general overview, a more detailed description can be found in Heikenfeld et al., (2019)):

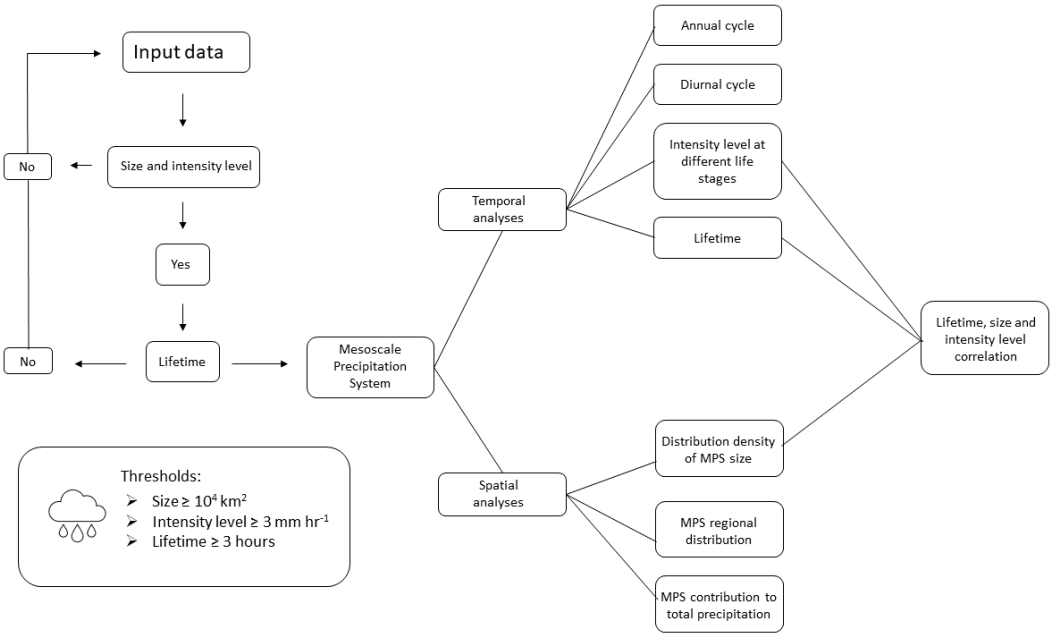

Figure 2- Work flow in identifying a Mesoscale Precipitation System (MPS), including the thresholds used for defining an MPS and the output analyses.

From the input data, the tobac algorithm will identify convective precipitation systems in the following two steps.

1. Identifying convective precipitation systems with an area $\geq 10^4$ km^2 and with a precipitation intensity of ≥ 3 mm hr^{-1}.
2. Identifying convective precipitation systems from step 1 which have a duration of ≥ 3 hours. If fulfilled, it is by definition an MPS and will be tracked.

By using the propagation speed from a detected convective precipitation system in step 1, the tobac algorithm calculates that system's possible future location. This ensures that, in step 2, it is an individual system that has been tracked over time which is defined as an MPS.

2.2.2 Life stages and precipitation intensity levels

We have chosen four life stages to study further: initiation, dissipation, max extension, and max intensity level.

Initiation is defined as the timing of the first identification of an MPS, while dissipation is defined as the timing of the last identification of an MPS. The max extension stage is defined as the timing of an MPS's reaching its largest size. Further, the precipitation intensity threshold for an MPS was also divided up in a total of eight intensity levels, ranging from 3 - >10 mm hr^{-1} (). This enables us to identify the various intensity an MPS can contain during a lifecycle. The timing of the highest intensity level during an MPS's lifecycle will be defined as its max intensity level.

2.3 Analyses

A summary of the analyses conducted, divided into their spatial or temporal nature, can also be seen in Fig. 2.

2.3.1 Focus months

To get an overview of the annual distribution of MPSs and in which months they usually are formed, we conducted an annual cycle with the number of MPSs in each month for the extensive domain. The results enabled us to identify the months when MPS formation dominated and remaining analyses included only MPSs of those months.

2.3.2 Temporal analyses

In order to understand the time of day when MPS convection was most active or passive in the two study regions, a diurnal cycle analysis was conducted based on tracked MPSs at every timestep of their lifecycle. This was done for both their hourly frequency as well as fraction.

We also calculated the number of MPSs based on their intensity level at different stages of an MPS's lifecycle. This was done in order to analyze which intensity level dominated during the different phases of an MPS. Following four different stages were chosen (see sect. 2.2 step 1-2 for further description): initiation, dissipation, max intensity level and max extension stage. We also analyzed the lifetime for each MPS by calculating the time passed between initiation and dissipation and plotted the distribution in each dataset using a boxplot.

2.3.3 Spatial analyses

The size of each MPS was provided by the tobac algorithm output in number of grid cells one MPS covered, which was then converted to km^2 based on the resolution of each dataset. For WRF_GU and HAR, the number of grid cells could be directly multiplied by their resolution. For GPM and ERA5, however, the data was provided with the resolution in degree at the equator. We therefore needed to weight the resolution for each latitude to get the most accurate size for each MPS. The results were analyzed using a histogram, which allowed us to look at the MPS size distribution in each dataset. In addition, to find out if there were any relationships between MPS characteristics (e.g. if larger MPSs had a higher intensity level or a tendency to last longer), we constructed a Spearman correlation matrix between MPS size, intensity level and lifetime.

We were also interested in where MPSs tended to form in order to understand their possible relationships to the regional climate. This was done by plotting the location of each MPS at their time of initiation over the extensive domain. In addition to the location of each MPS, we wanted to analyze how much precipitation MPSs contributed with to the total amount, in order to understand the magnitude of their influence on precipitation in the extensive domain. This was done by extracting precipitation within the extent of each identified MPS over the entire time period. The extracted precipitation was then used to calculate its fraction of the total precipitation. Finally, we also included an analysis to understand the precipitation patterns in the extensive domain by calculating the mean sum of precipitation for each year.

3 Results

3.1 Annual cycle

MPSs in the extensive domain between 2001 - 2016 mostly occurred during summer months (Fig. 3). They started to increase significantly in June, peaked in July and then decreased again. ERA5 had the most pronounced monthly fractional peak, followed by GPM and HAR while WRF_GU had the lowest. Additionally, while GPM, HAR and ERA5 all had a similar annual cycle, albeit some differences in their July peak, WRF_GU had a more smoothed annual cycle with higher monthly fraction of MPSs during winter and spring than remaining datasets. Still, all datasets showed a summer peak and analyses in this report will therefore focus on the months May to September (MJJAS).

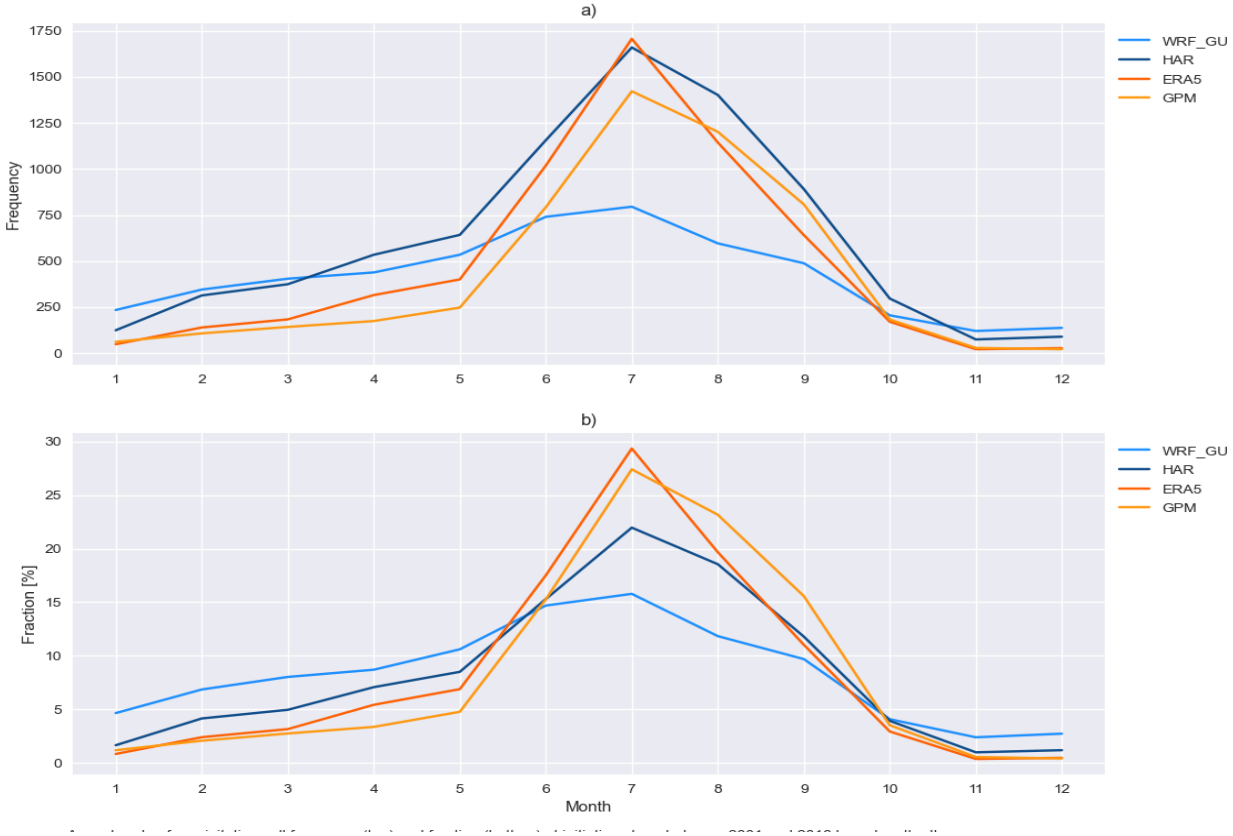

Figure 3. Annual cycle of MPSs monthly (a) frequency and (b) fraction at initiation stage between 2001 and 2016 based on the three model/reanalysis datasets (WRF_GU, HAR & ERA5) and the satellite dataset (GPM).

3.2 Number of tracked MPSs

In Table 1, the number of tracked MPSs during MJJAS are shown for the two study regions. In the extensive domain, WRF_GU was the dataset which detected least MPSs, while HAR detected the most. We can also see that in the TP domain, both RCM simulations WRF_GU and HAR were able to detect MPSs to a large extent. The one dataset of least detected MPSs in this

region was the global reanalysis dataset ERA5, beaten with around 200 MPSs by the satellite observations from GPM (Table 1).

Table 1. Total number of tracked MPSs in the two study areas: extensive and TP domain.

Dataset	Extensive domain	TP domain
WRF_GU	3153	1358
HAR	5751	1406
ERA5	4910	171
GPM	4472	367

3.2 Diurnal cycle

The diurnal cycle of MPS convection (i.e. MPSs at every timestep) in the extensive domain during MJJAS between 2001 – 2016 at local standard time (LST) can be seen in Figure 4. It shows that WRF_GU had the diurnal cycle with lowest frequency of MPS convection in nearly every hour, with the exception between 18.00 and 21.00 LST when ERA5 had a slightly lower frequency (Fig. 4a). In the hourly fraction diurnal cycle (Fig. 4b), WRF_GU and GPM peaked at laten night/early morning and reached their minimums around noon. HAR did also have a late night/early morning peak followed by a decrease, but it did not reach its minimum until late evening. In contrast to WRF_GU and GPM, HAR did not experience an equally distinct minimum and its MPS convection during a day was more smoothly distributed. ERA5 had a few hours later peak than remaining datasets and did not reach its minimum until late evening.

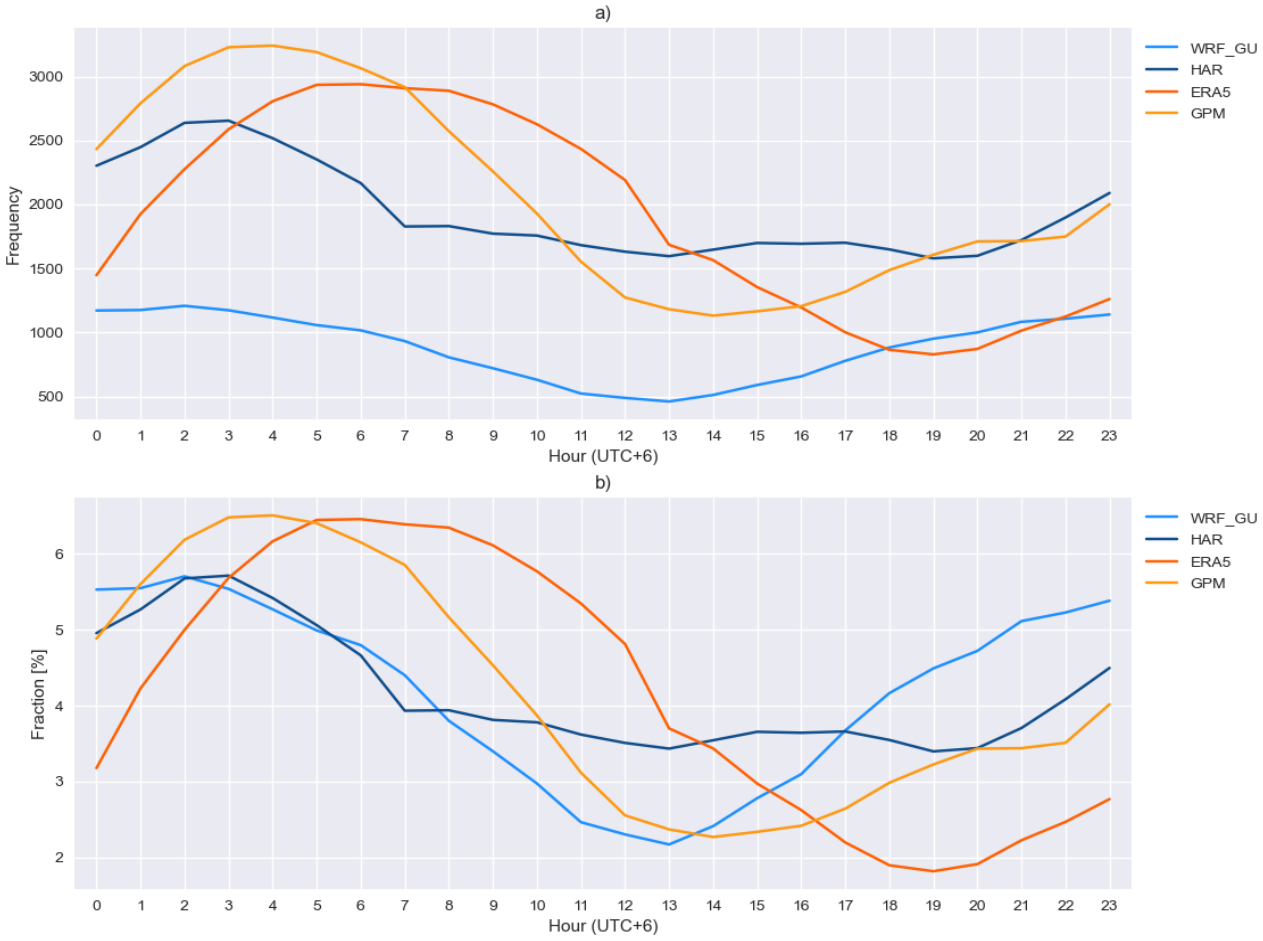

Figure 4. The diurnal cycle of MPS convection at every timestep of their lifecycle, including the hourly (a) frequency and (b) fraction in the extensive domain between 2001 and 2016. Data used were the three model/reanalysis datasets (WRF_GU, HAR & ERA5) and the satellite dataset (GPM).

In the TP domain, the hourly frequency diurnal cycle (Fig. 5a) showed that ERA5 had the lowest MPS convection in every hour, except during early to late morning when GPM had the lowest. WRF_GU and HAR both had higher frequencies than ERA5 and GPM in every hour. WRF_GU, GPM and HAR's hourly fraction diurnal cycles peaked during late evening and reached their minimum between late morning and noon (Fig. 5b). Due to the low frequency in every hour of ERA5, its hourly fraction diurnal cycle mainly constituted of irregularities (Fig. 5b).

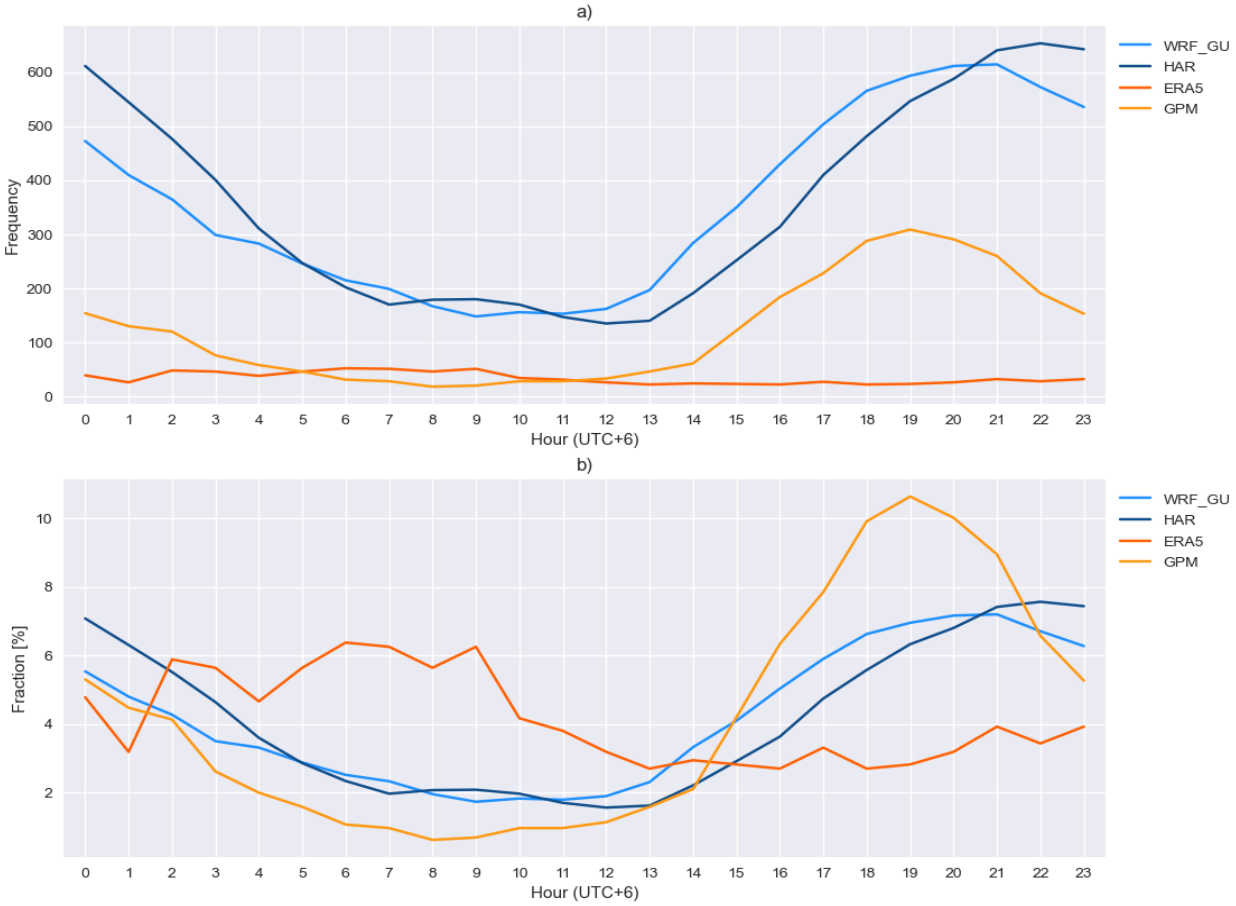

Figure 5. The diurnal cycle of MPS convection at every timestep of their lifecycle, including the hourly (a) frequency and (b) fraction in the TP domain between 2001 and 2016. Data used were the three model/reanalysis datasets (WRF_GU, HAR & ERA5) and the satellite dataset (GPM).

We did also conduct an hourly fraction diurnal cycle of MPS convection for each intensity level (see step 2 in sect 2.2.2) to investigate if a change in intensity level could impact the diurnal cycle. Each intensity level's diurnal cycle in the extensive domain can be seen in Figure 6 and it was detectable that, when moving towards an increasing intensity level, each dataset experienced a more pronounced diurnal cycle. Noticeable also is how similar diurnal cycles HAR and GPM have in intensity level 10, where both have the same timing in both increase and decrease although their actual peak differs somewhat. No pattern could not be detected in the TP domain (figure not shown).

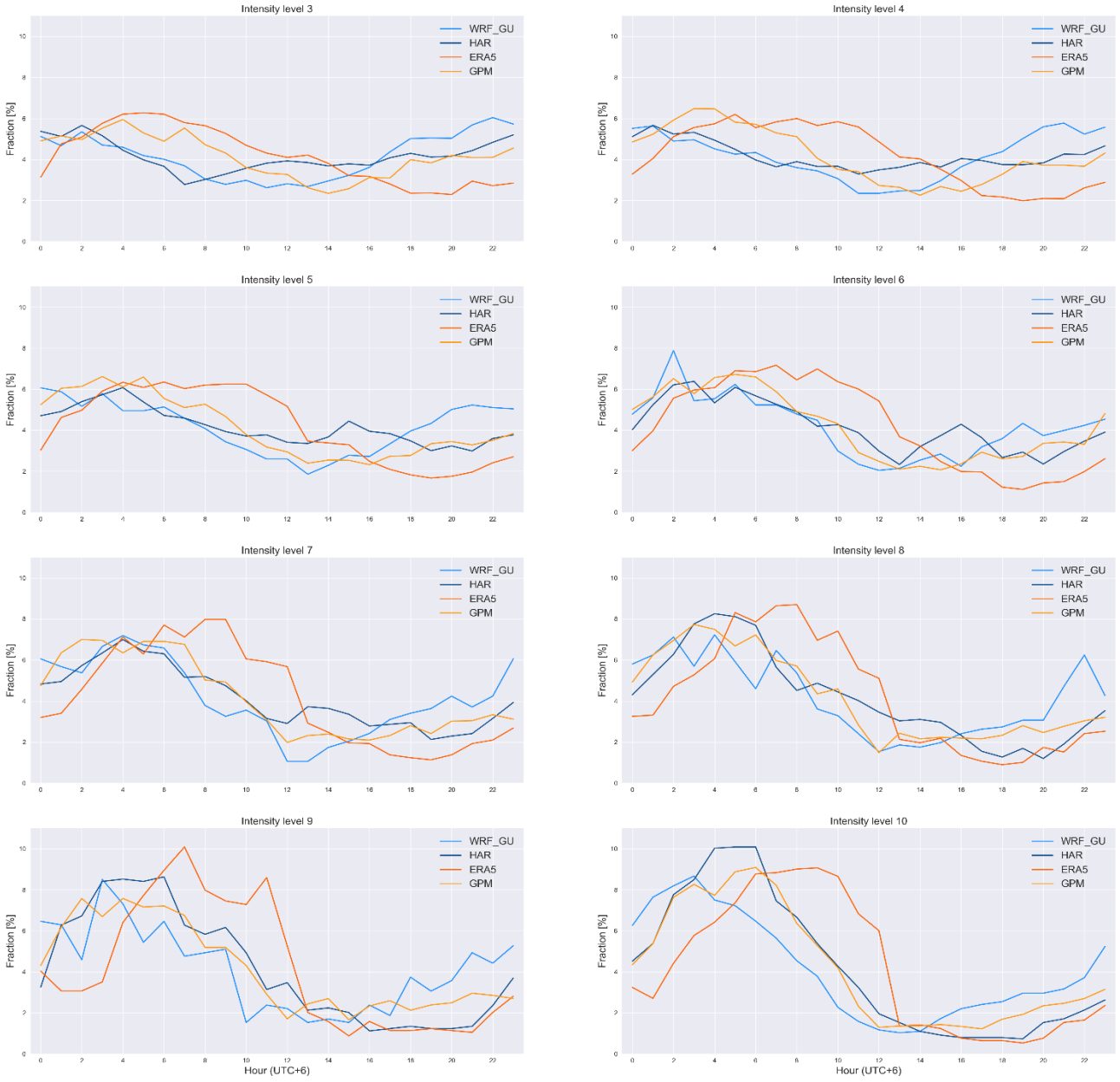

Figure 6. The diurnal cycle of MPS convection at every timestep of their lifecycle. It regards the hourly fraction in the extensive domain for each intensity level [mm h^{-1}] between 2001 and 2016. Data used were the three model/reanalysis datasets (WRF_GU, HAR & ERA5) and the satellite dataset (GPM).

3.3 Intensity level at different life stages of MPSs

The extensive domain results showed that all datasets during initiation, dissipation and max extension stage had a similar pattern with most MPSs at intensity level 3, although max extension stage had a slightly more smoothed distribution (Fig. 7 a, b, d). At max intensity level stage (Fig. 7c), the distribution was more evenly distributed with most MPSs at intensity level 4 (WRF_GU, HAR, ERA5) and intensity level 10 (GPM) instead. Although all datasets had higher fractions of intensity level 10 at max intensity level stage, WRF_GU and GPM stood out with around 18 and 22% respectively. Additionally, at all stages, a similar pattern of distribution was found between WRF_GU-GPM and HAR-ERA5 (Fig. 7a - d). These results were similar to those in the TP domain (figure not shown).

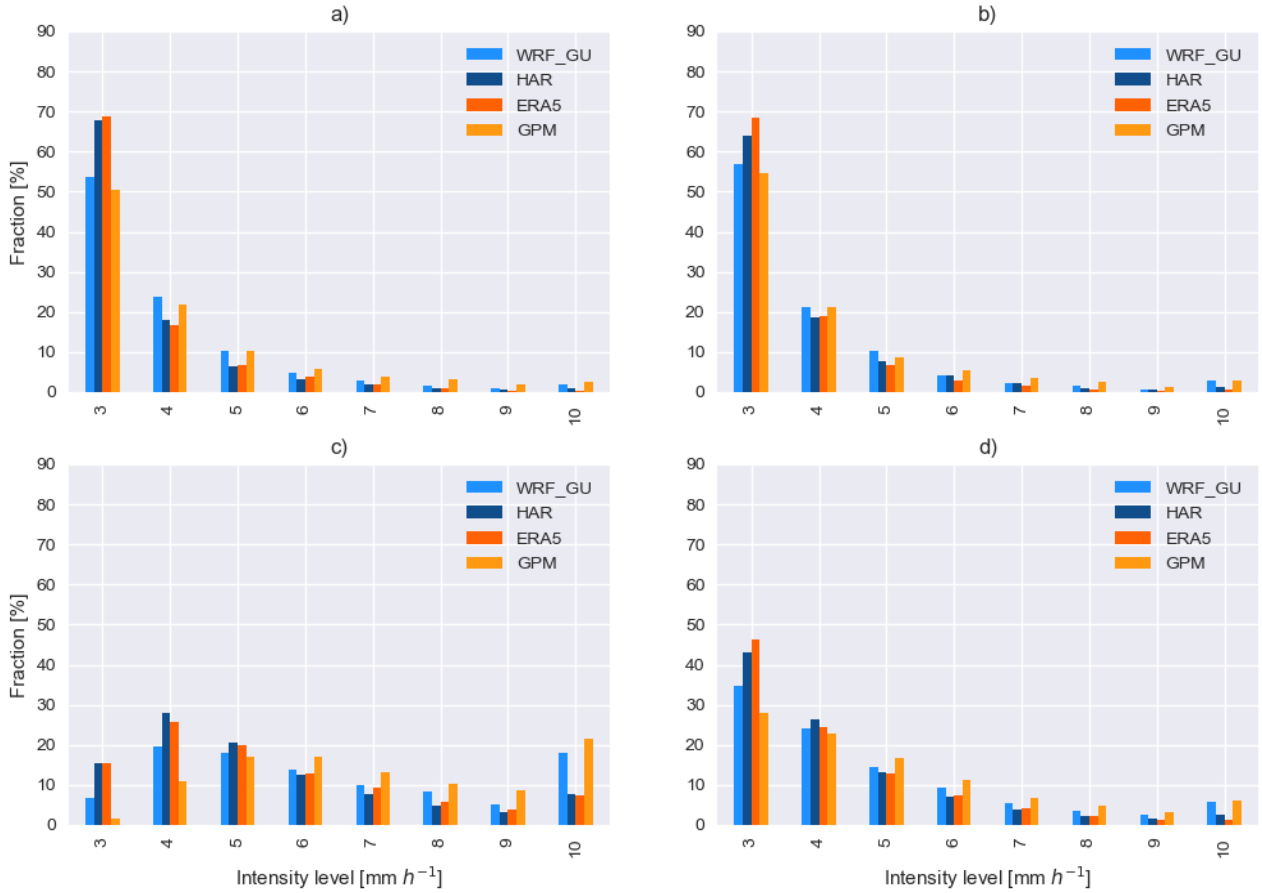

Figure 7. Intensity level fraction of MPSs at (a) initiation, (b) dissipation, (c) max intensity level and (d) max extension stage based on the three model/reanalysis datasets (WRF_GU, HAR & ERA5) and the satellite dataset (GPM).

3.4 Lifetime

Figure 8 shows a boxplot of each dataset's MPS lifetime distribution in the two study regions. In the extensive domain (Fig. 8a), WRF_GU and GPM had the most concentrated distributions. GPM had the lowest median of 4.5 hours, ERA5 and HAR

the highest of 6 hours, while WRF_GU had a median of 5 hours. In contrast to the extensive domain, WRF_GU had the least concentrated distribution in the TP domain (Fig.8b), while GPM still had the most concentrated. For HAR and ERA5, both had a more concentrated distribution than in the extensive domain. While WRF_GU had the same median as in the extensive domain, remaining datasets experienced a decrease.

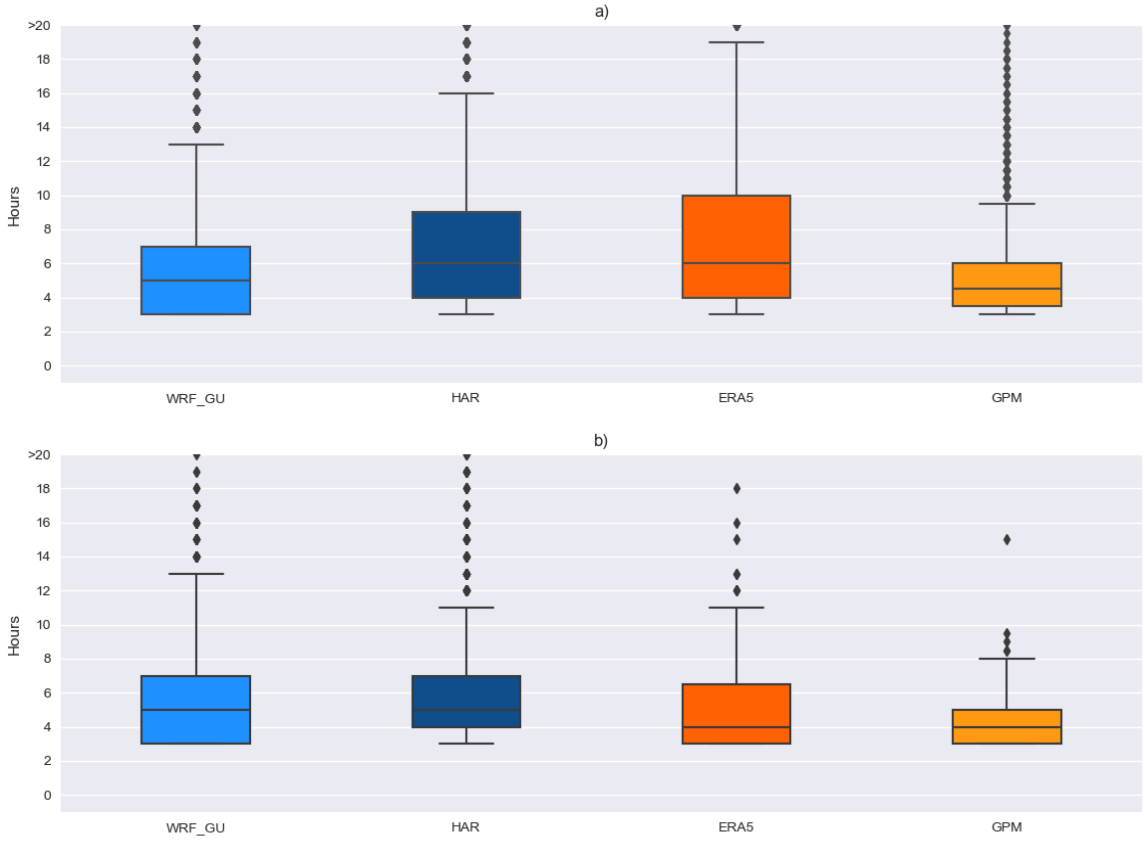

Figure 8. Boxplot of MPSs lifetime in the (a) extensive domain and (b) TP domain based on the three model datasets (WRF_GU, HAR & ERA5) and the satellite dataset (GPM).

3.5 Size distribution density of MPSs

Figure 9 consists of a histogram with the fraction of MPSs at every 10^4 km^2 in the extensive domain. The results showed that HAR and GPM had the most similar extension distribution curve with their largest MPSs between $2x10^4$ - $6x10^4$ km^2 (Fig. 9b, d). WRF_GU resulted in slightly smaller MPSs with a distinct peak between 10^4– $4x10^4$ km^2 (Fig. 9a) while ERA5 peaked at $10x10^4$ km^2, had larger MPSs overall and a smoother distribution (Fig. 9c). These results were similar to those in the TP domain (figure not shown).

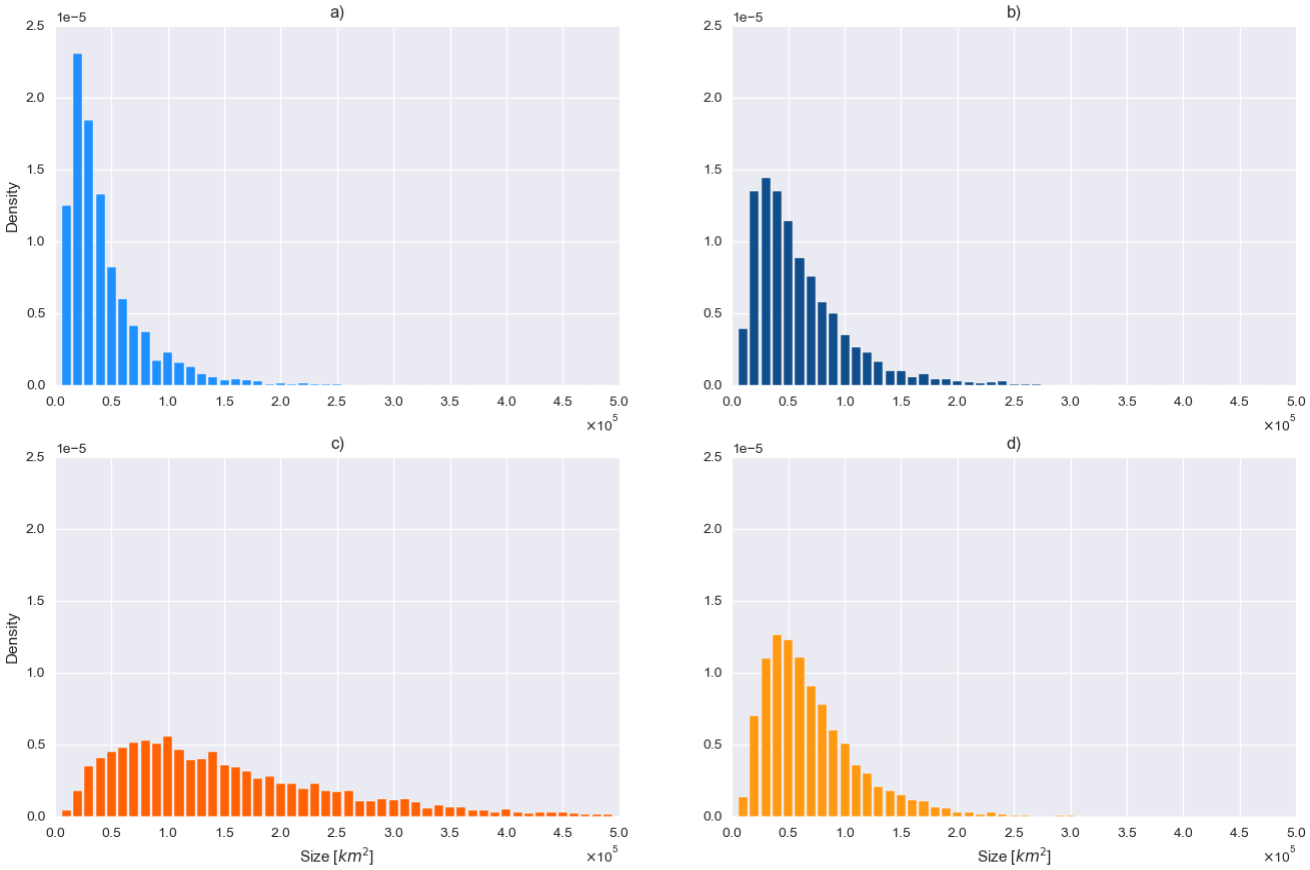

Figure 9. Distribution density of MPSs size at initiation stage in the extensive domain based on (a) WRF_GU, (b) HAR, (c) ERA5 and (d) GPM.

3.6 Relationship between lifetime, extent, and intensity level

The correlation matrices for the extensive and TP domain are shown in Figure 10 and 11 respectively. In the extensive domain, HAR and ERA5 had the highest correlations between MPS lifetime and intensity level, followed by GPM and lastly WRF_GU (Fig. 10). All datasets experienced a low correlation between MPS lifetime and size, although HAR's was almost at a modest level. A similar pattern could be stated in the MPS intensity level and size correlations. All correlations were statistically significant at the confidence level $p < 0.005$.

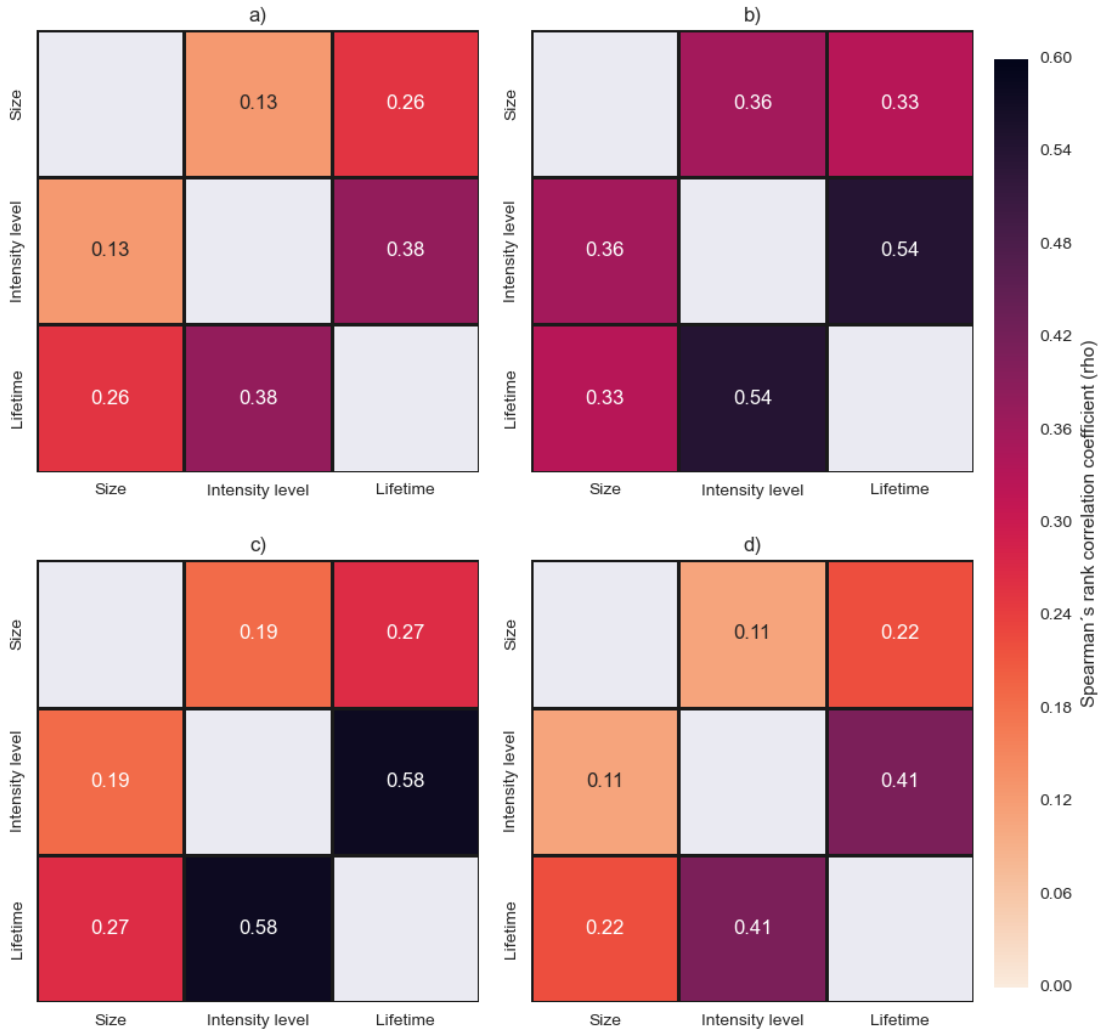

Figure 10. Spearman's rank correlation matrix of MPS size, intensity level and lifetime in the extensive domain based on (a) WRF_GU, (b) HAR, (c) ERA5 and (d) GPM. Darker colors are coupled with a higher rho value (Spearman's rank correlation coefficient)

As for the extensive domain, MPS intensity level and lifetime correlations in the TP domain resulted in the highest correlations. This time, however, HAR and WRF_GU had the highest correlation coefficients (Fig. 11). WRF_GU did also result in the same correlation coefficient regarding MPS lifetime and size as in the extensive domain (Fig. 11b). All correlations for WRF_GU and HAR were statistically significant at the confidence level $p < 0.05$. The MPS lifetime and intensity level correlations of GPM and ERA5 were both statistically significant at the confidence level $p < 0.05$, their remaining correlations were not.

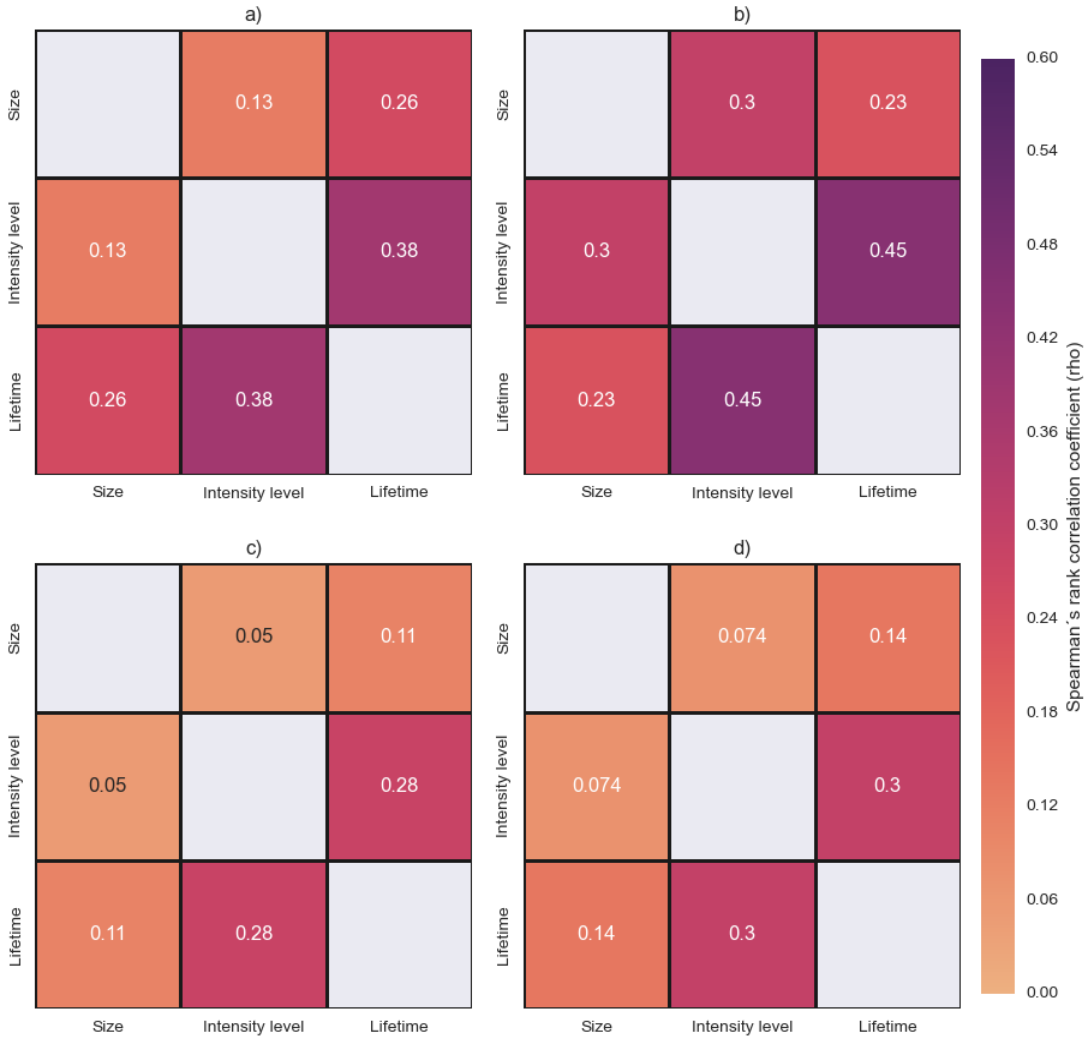

Figure 11. Spearman's rank correlation matrix of MPS size, intensity level and lifetime in the TP domain based on (a) WRF_GU, (b) HAR, (c) ERA5 and (d) GPM. Darker colors are coupled with a higher rho value (Spearman's rank correlation coefficient)

3.7 Spatial density of MPSs

In Figure 12, the density of tracked MPSs at initiation stage can be seen. Of all datasets, WRF_GU had the overall lowest density of MPSs (Fig. 12a). WRF_GU and HAR had higher MPS density over the TP than ERA5 and GPM, both with highest densities at the eastern TP (Fig. 12a - b). HAR, ERA5 and GPM all had a high MPS density south of the TP southern border with over 200 MPSs in a large part, especially southeast of the TP (Fig. 12b - d).

‘

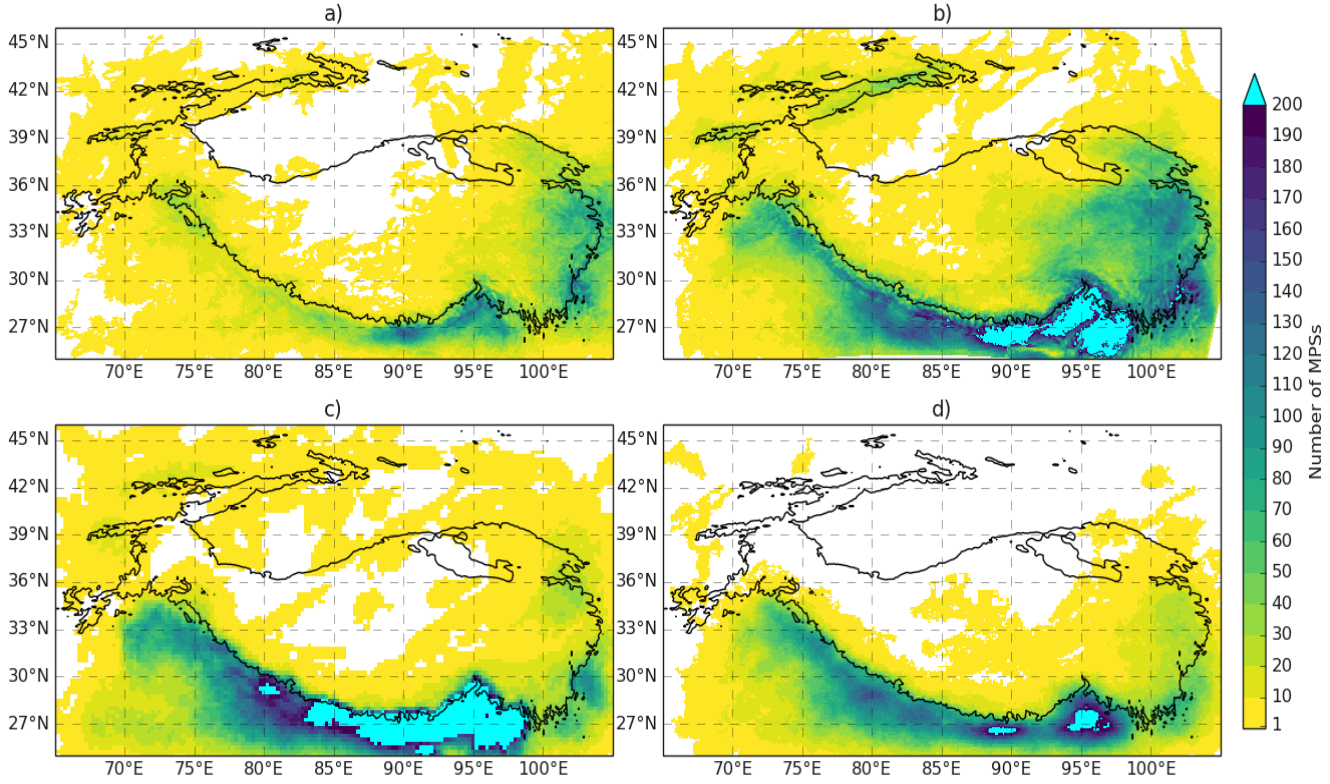

Figure 12. MPSs spatial density (number of tracked MPSs in each grid cell) in the TP region for (a) WRF_GU, (b) HAR (c), ERA5 and (d) GPM at initiation stage between 2001 – 2016 (white areas = no MPSs at initiation stage).

3.8 Total precipitation & MPSs contribution to total precipitation

The mean MJJAS sum of precipitation can be seen in Figure 13, while MPSs contribution to total MJJAS precipitation can be seen in Figure 14. In all four datasets, the highest mean MJJAS sum of precipitation was concentrated in the southeastern area of the TP region (Fig. 13a - d). ERA5 and HAR had the largest areas of highest precipitation, extending along the Himalayan mountain range. WRF_GU, HAR and ERA5 all reached above 5000 mm, while the max precipitation of GPM remained below. Finally, on the TP, ERA5 had the overall highest amount of precipitation, followed by HAR and lastly WRF_GU and GPM (Fig. 13a – d).

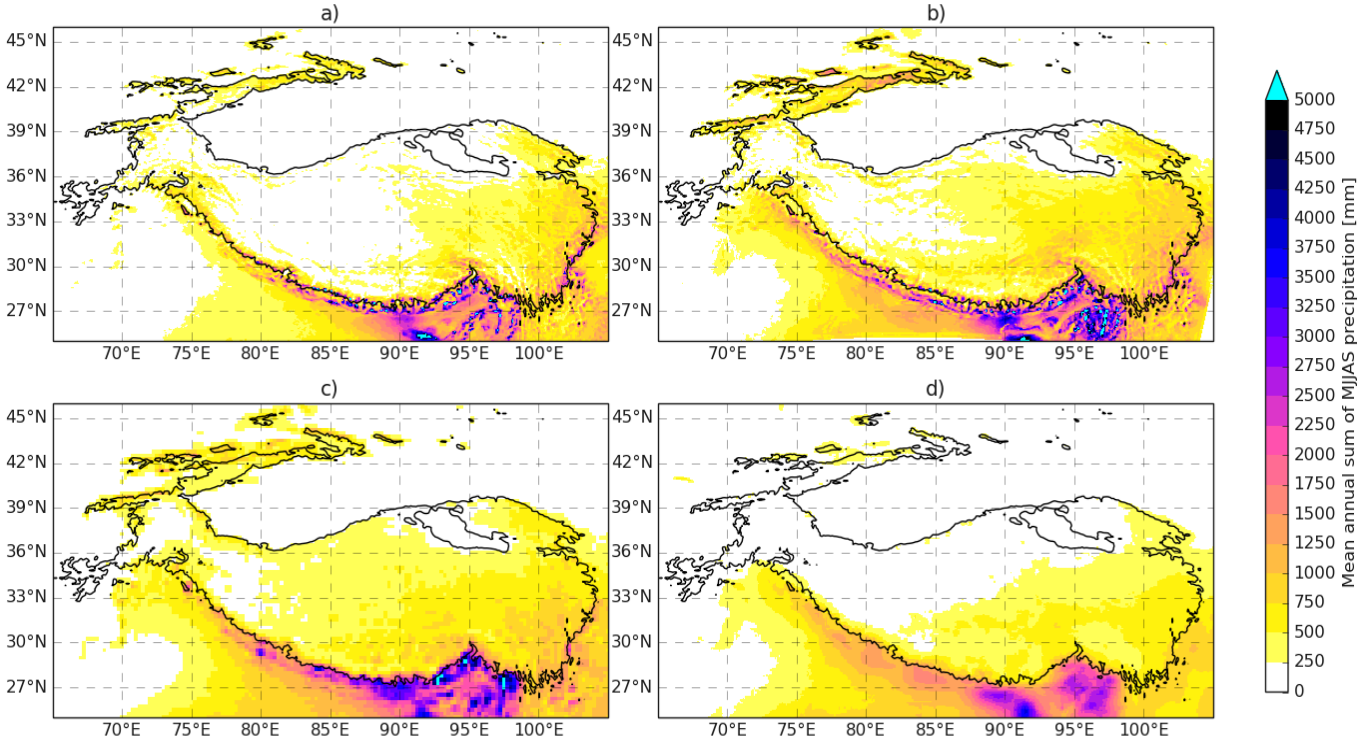

Figure 13. Mean May – September (MJJAS) sum of precipitation in the TP region for (a) WRF_GU, (b) HAR, (c) ERA5 and (d) GPM between 2001 - 2016. All areas have precipitation above 0mm.

GPM had the overall lowest contribution from MPSs to total MJJAS precipitation (Fig. 14d), followed by WRF_GU (Fig. 14a), ERA5 (Fig. 14c) and HAR (Fig. 14b). All datasets had a high contribution of precipitation along the southern TP border, although HAR and ERA5 had the highest. In HAR and ERA5, MPSs contribution also stretched across the southern TP border on to the TP (Fig. 14b, c), while WRF_GU and GPM were mainly south of the TP border (Fig. 14a, d). Both HAR and WRF_GU resulted with MPS contribution along the eastern side of the TP stretching westwards, where HAR had the highest MPS contribution (Fig. 14a, b). ERA5 and GPM both had sparse MPS contribution on the TP and to the eastern border of the TP (Fig. 14c, d).

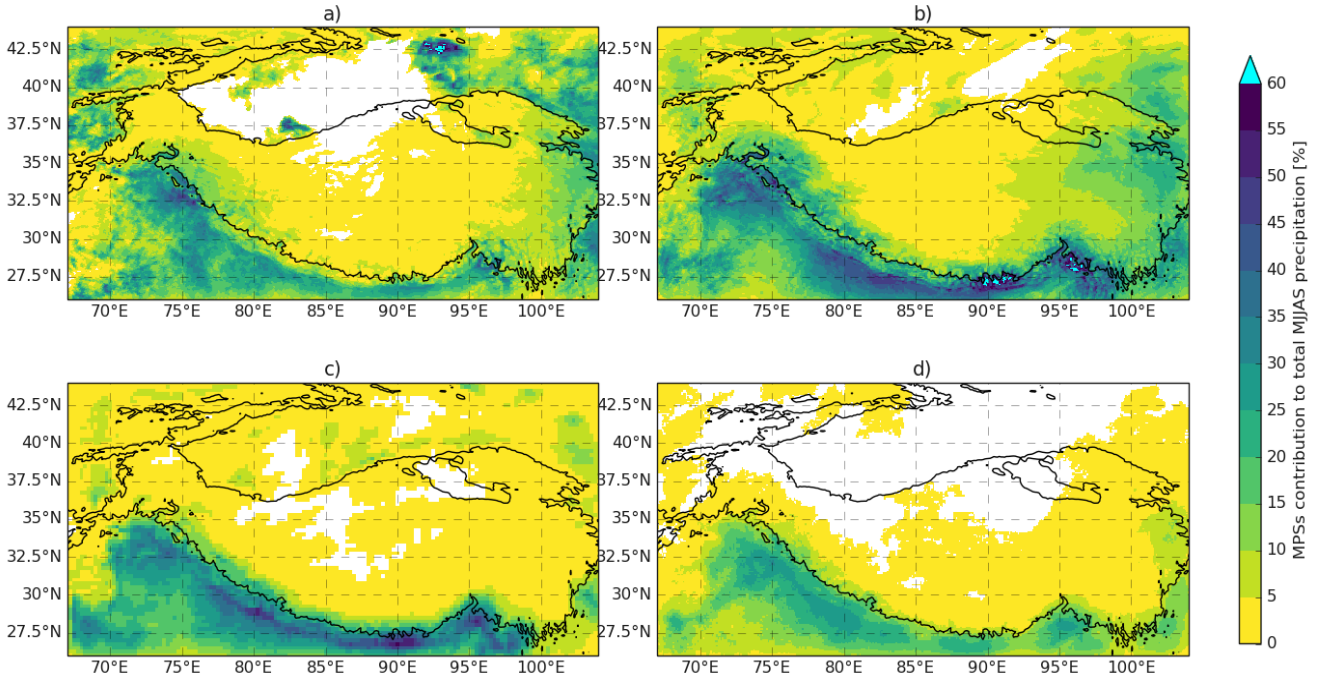

Figure 14. Contribution from MPSs to the total May – September (MJJAS) precipitation in the TP region for (a) WRF_GU, (b) HAR, (c) ERA5 and (d) GPM between 2001 - 2016 (white areas = no MPSs).

4 Discussion

4.1 MPSs formation and distribution

4.1.1 Orographic forcing and nocturnal cooling

Based on the results, some interesting characteristics for MPSs and their attributes in the region and TP domains between 2001 - 2016 were detectable. In the extensive domain, MPS convection in all datasets tended to peak in early morning and decrease during late morning and midday hours (Fig. 4). Convective precipitation systems in this region have been shown to vary greatly in scale, all contributing significantly to the total precipitation. They have also been shown to be highly affected by different regional climate and topographic properties such as orography and daytime solar heating/nocturnal cooling depending on their origin (Medina et al., 2010; Romatschke & Houze, 2011). It is therefore complicated to assign one reason for the early morning peak, as it is rather a question of a multiple processes, but oceanic moisture is often involved. In a report by Romatschke & Houze, (2011), they studied the initiation of convective precipitation systems and their contribution to precipitation during the South Asian Monsoon (SAM). They used three different scales to define the various convective precipitation systems: small (600 - 10^4 km^2), medium (10^4 - 4.4x10^4 km^2), and large (> 4.4x10^4 km^2). Their analyses focused on the TP with surroundings using the NCEP/ NCAR reanalysis data. In their results, a nocturnal triggering of precipitation over the Bay of Bengal (BoB)

produced heavy rainfall between midnight and noon. Due to the southwesterly wind flow pattern characteristic for the SAM in the southern TP region, moist air from the BoB was transported towards the southeastern TP where it was forced orographically and enabled a triggering of convection, mainly at night and of medium size (Medina et al., 2010; Romatschke & Houze, 2011). A similar pattern has also been shown to occur in the southwestern TP area but with moist air originating from the Arabian Sea instead (Medina et al., 2010; Romatschke & Houze, 2011; Ye & Wu, 1998). Additionally, daytime solar heating enables a strong convergence over the TP triggering convection of small-scale precipitation systems as warm moist air is being orographically lifted along the Himalayan mountain range (Romatschke & Houze, 2011). During nighttime, however, the effect is reversed as the TP air cools down and flows downslope instead. As a result, convection of precipitation systems along the Himalayan foothills will occur as the cool air converges with moist air from lower altitudes (Houze, 2012). These convective precipitation systems have been identified to form from midnight to early morning and being of medium rather than small scale (Romatschke & Houze, 2011).

Both the southeastern and southwestern TP orographic forcing and Himalayan nocturnal cool air effects are interesting since they are coherent with our results on several points. First, except for ERA5, the defined range for medium sized convective precipitation systems (10^4 - $4.4x10^4$ km^2) by Romatschke & Houze, (2011) was also the most common size range of our tracked MPSs at initiation stage (Fig. 9). The timing of both these effects in triggering convection did also match the diurnal peaks of MPS convection in our results (Fig. 4). Finally, the MPSs were located in areas where the results of both mean MJJAS sum of precipitation (Fig. 13) as well as MPS density (Fig. 12), in all datasets but WRF_GU, were intense. These results suggest that our tracked MPSs are coherent with the convective and precipitation patterns characteristic for the SAM discussed by Romatschke & Houze, (2011). The results also highlight the influence of mountain ranges on convective dynamics and how they can trigger convection of various sizes throughout a day.

4.1.2 Solar heating

In the TP domain, the diurnal cycle of MPS convection shifted towards an evening peak and early morning decrease instead, although with the exception of ERA5 (Fig. 5) which registered very few MPSs in this study region. The reason for this afternoon/early evening peak in MPS convection could be due to the pattern of convection development over the TP. By using active and passive remote sensing techniques in field experiments, Liu et al., (2015) analyzed diurnal variations of cloud properties in Naqu, an area located at the TP known for cloud formation. Their results showed that most clouds in this area formed after midday, especially between late afternoon and early morning, and mainly by strong surface heating which created a convergence zone that enabled convection (Liu et al., 2015; Romatschke & Houze, 2011). This is interesting in context to our findings since this timing matches the diurnal cycle of MPS convection results in the TP domain. However, while various regional climate effects could impact the diurnal cycle of MPSs at lower altitudes, as discussed for the extensive domain above, convection formation on the TP seems to be mainly affected by the daytime solar heating. Because, although WRF_GU and HAR resulted in relatively higher intensities of MPSs density and mean MJJAS sum of precipitation in the area of high

convection rates shown by Liu et al., (2015), the results of GPM did not (Fig. 12 & 13). Those results did rather have quite low overall intensity of both MPS density and mean MJJAS sum of precipitation in the TP domain but still a very distinct diurnal cycle (Fig. 5). This strong relationship between convective precipitation systems formation and daytime solar heating has also been concluded to result in a very distinct diurnal cycle, characterized by an afternoon peak and post-midnight decrease (Liu et al., 2015). These timings of peak and decrease are further argued by Yaodong et al., (2008) to be the most important results proving that daytime solar heating is the most dominating trigger of precipitation convection formation over the TP (Hu et al., 2016; Liu et al., 2015; Yaodong et al., 2008; Ye & Wu, 1998). Our results, therefore, add further validation to this argument.

4.1.3 What impacts precipitation intensity

Another interesting result was the distinct pattern of a more pronounced diurnal cycle towards a higher intensity level (Fig. 6). The regional climate effects enabling the formation of MPSs discussed above produce medium to large scale level systems ($>10^4\,km^2$) (Romatschke & Houze, 2011). Although large systems can produce heavy rainfall and, thereby, contribute largely to total precipitation (Houze Jr, 2004; Romatschke & Houze, 2011), smaller scale systems also play an important role due to their high frequency of occurrence (Romatschke & Houze, 2011). It has also been shown that a more pronounced diurnal cycle often is characteristic with larger convective precipitation systems, while smaller and, to some extent, medium systems have the tendency to be produced throughout the day (Romatschke & Houze, 2011). It would therefore seem reasonable to find a positive correlation between MPS size and intensity level. However, HAR was the only dataset which resulted in a moderate correlation between the two (Fig. 10). There was also no clear relationship found when analyzing the distribution of MPSs at max extension stage binned by each intensity level (Fig. 7). These two results suggest that intensity level had a closer relationship to other factors than the actual size of an individual MPS. Because, in a report by Houze Jr et al., (2007) analyzing monsoon convection in the Himalayan region, they too could conclude that moist Arabian Sea and BoB air was forced to intense convection by orographic lifting along the Himalayan foothills. The full effect of the convective precipitation systems resulting precipitation and size, however, mainly occurred in the stratiform rather than in the deep convection part. In their case, this meant that the largest and most intense precipitation regions of the convective precipitation system were located further south of the Himalayan mountain range, rather than over the high terrain (Houze Jr et al., 2007). Now, in our results, although WRF_GU and GPM had a modest correlation between lifetime and intensity level, HAR and ERA5 had quite high correlations between the two (Fig. 10). They were also the two datasets with overall longest lifetime of MPSs in the larger extensive domain (Fig. 8). In context to the findings of Houze Jr et al., (2007), this could mean that the longer lived MPSs identified in our results develop a region of intense precipitation distanced from the high terrain areas, since MPS initiation was most intense over the Himalayan mountain range but still with a high contribution to MJJAS precipitation stretching southwards. These results also suggests that lifetime is more important for the intensity level rather than the actual size of an MPS.

Additionally, the areas of high MPS density identified in our results have been located in high terrain regions impacted by moist air from the Arabian Sea (southwestern TP) and BoB (southeastern TP) (Medina et al., 2010; Romatschke & Houze, 2011; Ye & Wu, 1998). It has also been shown by previous research that convective precipitation systems in these regions experience a distinct diurnal cycle similar to our results (Houze, 2012; Medina et al., 2010; Romatschke & Houze, 2011). Our results, therefore, suggests that these MPSs might contain a high intensity level but still be of various size and that regional patterns and lifetime play an important role on an MPS's intensity level. The importance of lifetime also became evident in the TP domain relationship between lifetime, extent, and intensity level correlations (Fig. 11). First, relative to the extensive domain, all datasets except WRF_GU experienced a decrease in their MPS lifetime and intensity level correlations and, secondly, all datasets except WRF_GU did also have an overall shorter lifetime of their MPSs. These findings, therefore, further argues for the importance of lifetime on an MPS's intensity level.

4.2 Spatial resolution and early convection

4.2.1 Unstable stratification

Of the three model datasets used, ERA5 had the lowest spatial resolution. This became evident in the MPS size results where ERA5, compared to GPM, was not able to detect smaller systems to the same extent as WRF_GU and HAR but rather more prone to detect the opposite (Fig. 9). We could also see that ERA5 detected fewer MPSs in the smaller TP domain than remaining datasets (Table 1). Since the two downscaled regionally climate model simulations (WRF_GU and HAR) were driven by ERA5, these results suggest that they can bring an added value in analyzing MPSs on a wider scale in mountainous areas such as the TP region.

Unstable stratification has been shown to be the main cause of convection initiated over the TP due to the strong surface heating (Hu et al., 2016; Liu et al., 2015; Yaodong et al., 2008; Ye & Wu, 1998). This might also explain ERA5's lesser ability to detect smaller MPSs. As discussed by Sato et al., (2008), lower spatial resolution datasets (≥28 km grid size) are too coarse to detect initial convection in areas of unstable stratification. They further argue that this causes a delay in the diurnal cycles of convective precipitation systems, as they are registered in a later phase of their lifecycle (Sato et al., 2008). This was also evident in our results, where MPSs tracked using ERA5 experienced a delayed diurnal cycle compared to remaining datasets. It was also evident in our results that the overall lifetime of MPSs in the TP domain were shorter (Fig. 8), coherent with previous research as well (Hu et al., 2016; Mai et al., 2021; Sato et al., 2008), and that MPSs in the ERA5 results were overall larger (Fig. 9). Now, as convective precipitation systems mature, they tend to stretch and reach a larger horizontal scale since stratiform clouds develop at the top (Houze Jr, 2004; Romatschke & Houze, 2011; Sato et al., 2008). The generally lower lifetime of MPSs in the TP domain might, therefore, be too short for MPSs to develop and reach a horizontal scale large enough for ERA5 do detect. This argument is further strengthened by the fact that convection in ERA5 was delayed compared to remaining datasets and that its MPSs were the largest.

It should also be highlighted that, although MPSs subset by the TP domain have lasted ≥ three hours and that some MPSs were identified to have been initiated over the TP, we have not conducted an analysis of their movements. This could mean that MPSs detected by ERA5 in the TP domain might have been initiated outside the plateau, thus being MPSs at a mature stage with a larger horizontal scale. This assumes that ERA5 does not detect early convection, otherwise it could be the opposite pattern with MPSs at an early lifecycle stage. Further research is therefore needed for a conclusion in the matter.

4.2.2 Topographic features

The ERA5 diurnal cycle of MPS convection s in the TP domain was quite distinct to remaining datasets (Fig. 5). Due to the low number of detected MPSs (Table 1), drawing any major conclusions from its diurnal cycle might therefore be debatable. However, in the extensive domain, ERA5 detected a relatively large number of MPSs (Table 1) which experienced a delay relative to remaining datasets in its diurnal cycle (Fig. 4). This might be an effect of spatial resolution because, in the report by Sato et al., (2008), they also found a relationship between stronger convergence and increased resolution due to the enhanced topographic details in such datasets. This could be shown both over the TP and the Himalayan mountain range where convergence was strong in their higher resolution datasets (≤ 7 km), weak in the medium resolution dataset (14 km) and absent in the course dataset (28 km). Both the medium and course datasets did also result in a three hour delay of cloud formation (Sato et al., 2008), similar to our results where MPS convection in ERA5 peaked two and three hours later than the high resolution datasets of WRF_GU and HAR respectively. This indicates that early convection is not only delayed in areas of unstable stratification but also where orographic lifting occurs. As a result, ERA5 registers MPS convection at a later stage also in the larger extensive domain than WRF_GU and HAR, causing a delay in its diurnal cycle and overall larger MPSs. The importance of topographic features as represented by datasets with various spatial resolutions and its impact on convection and precipitation have also been shown in results by numerous other researchers focusing on various regions of the world (Lin et al., 2018; Prein et al., 2013; Wagner et al., 2018; Zhao et al., 2021).

4.3 Effect of convective parameterization

In addition to a better topographic representation, higher spatial resolution also enables model runs without convection parameterization (CP) schemes. In this report, WRF_GU was the only dataset where CP was switched off in the model run and it was quite distinct to HAR and ERA5 in the number of MPSs detected in the extensive domain (Table 1). In a study by Zhao et al., (2021), a 13 km horizontal grid CP model simulation (LSM) was compared to a 4 km horizontal grid convection-permitting model simulation (CPM) over the TP. They found an overestimation of convection in the LSM and argued that the CP could be the main cause rather than resolution itself, although a high enough resolution is needed to turn off parameterization (Zhao et al., 2021). This argument has also been raised in a study by Pearson et al., (2014) who analyzed tropical convection in West Africa. Their results showed that a 12 km model simulation without CP outperformed a 1.5 km simulation in total cloud fraction when compared to an observational dataset (Pearson et al., 2014). The findings of excessive

convection when using a parameterized convection scheme by Zhao et al., (2021) also showed to cause a wet bias of precipitation over the TP. Similar results were also presented by the producer of the WRF_GU dataset, where precipitation was better represented by the non-convective parameterization simulation compared to observational data (Ou et al., 2020). These findings are interesting in context to our results since we also saw a quite large distinction of MPS number and density between non-parameterized convection simulations (WRF_GU) and parameterized convection simulations (HAR and ERA5), with overall lower values of the former. Although not as distinct, differences could also be seen in the mean MJJAS sum of precipitation results with higher and more widespread values of HAR and ERA5 on the TP as well as south of the Himalayan mountain range (Fig. 13).

Additionally, of our model simulation results, WRF_GU had a general tendency to better match the observational dataset of GPM in several statistics in the extensive domain such as the relationship between lifetime, extent, and intensity level correlations (Fig. 10), diurnal cycle (Fig. 4), and lifetime (Fig. 8). They also had a similar distribution of MPSs within each intensity level, both with a better representation of higher threshold values (Fig. 7). On the other hand, MPSs size (Fig. 9) and the diurnal cycle of intensity level 10 (Fig. 6) were two exceptions where HAR and GPM had a closer match. These results, therefore, suggest that a non-parameterized convection simulation model dataset could represent MPSs and their characteristics in the extensive domain better than one using parameterized convection, but that uncertainties remain. What we could see, however, was that CP seems to have caused excessive convection as both HAR and ERA5 resulted in a higher number of MPSs compared to GPM, while the non-CP simulation of WRF_GU resulted in the opposite. It is uncertain why WRF_GU resulted in much fewer MPSs, one reason could be that, although it has CP turned off and previous research has argued for its benefit (Pearson et al., 2014; Zhao et al., 2021), it is still at the top boundary of the gray-zone in climate modelling and using a spatial resolution closer to 4 km could possibly be more accurate. Further research including such simulation might therefore be needed for a conclusion in the matter.

4.4 Spectral nudging vs re-initialization

The difference in MPS density between WRF_GU and HAR might also be related to whether spectral nudging (WRF_GU) or re-initialization (HAR) has been used in the model simulation runs, two techniques widely used in regional climate model downscaling to restrict the model runs from drifting too far away from the large-scale circulations (Bowden et al., 2012; Lo et al., 2008; Ma et al., 2022; Von Storch et al., 2000; Waldron et al., 1996). We found an overall higher density of MPSs in the HAR results compared to WRF_GU, especially along the Himalayan mountain range and on the eastern TP, but also over the TP as a whole. The MPS density of HAR was also shown to be overall much higher and widespread than the satellite observations of GPM, while the WRF_GU results, with the exception at the eastern TP, were slightly lower (Fig. 12). In a recent study by Ma et al., (2022), two regional climate simulations were compared, one using spectral nudging (EXP-SN) and the other re-initialization (EXP-RI). They were both driven by ERA5, simulated with the WRF model and at convective-permitting scale to avoid possible errors from using CP (Ma et al., 2022). In their results, the southeastern TP and its southern

slopes experienced intense convergence in both model runs, however stronger in the EXP-RI results. They also found stronger convergence over the central, central-eastern, and southeastern TP along with higher precipitation values in the EXP-RI compared to EXP-SN. It should be highlighted that they focused on convergence with a much finer resolution and direct comparison should therefore be done with care. Still, as convergence is highly involved in the convection process (Crook & Moncrieff, 1988), it is interesting in context to our results and the better representation of convergence shown by Ma et al., (2022) when using spectral nudging argues for its benefit.

According to Song et al., (2011), spectral nudging can also reduce errors caused by CP. They focused on summer precipitation in East Asia using the State University-National Center for Atmospheric Research Mesoscale Model driven by the National Centers for Environmental Prediction - National Center for Atmospheric Research (NCEP - NCAR) reanalysis data for the large-scale circulations. Their results showed that, when enabling spectral nudging in the model run, it decreased errors in large scale upper and lower atmospheric wind flows, resulting in a better representation of precipitation (Song et al., 2011). The atmospheric wind flows of concern were the upper westerly jet and the monsoonal southwesterly winds which transports moist air from the BoB to East Asia (Song et al., 2011). As both these wind flows have been shown to have a large impact on MPSs and precipitation of our results in the extensive domain, the findings of Song et al., (2011) further adds validity to using the spectral nudging technique. Still, based on our spatial distribution of MPSs and mean MJJAS sum of precipitation results (Fig. 12 & 13), it cannot be concluded which of WRF_GU and HAR better represent that of GPM and, therefore, we are not able to conclude if spectral nudging or re-initialization is preferred in this particular case. The re-initialization datasets did, however, both use CP and the combination seems to cause excessive triggering of convection while the opposite could be concluded for a non-CP simulation using spectral nudging at a spatial resolution of 9 km.

4.5 Importance of MPSs

The majority of the tracked MPSs were located in the most densely populated areas, mainly in northern India just south of the Himalayas (Fig. 12). This is also one of the most vulnerable regions to water stress, as there is a high freshwater and irrigation demand. With the population projected to increase significantly by 2050, this would further increase the water demand (Immerzeel et al., 2019). Much of the freshwater supply in this region originates from the TP glaciers but also from convective precipitation systems during the monsoon season (Yao et al., 2022). Due to temperature changes over the TP, the glacial meltwater supply has decreased rapidly simultaneously as the temperatures also have caused the Indian monsoon to weaken. This has resulted in a non-sufficient supply of freshwater from glacial meltwater, which is not counterbalanced by precipitation from convective systems (Yao et al., 2022). It has also been projected that temperatures will increase further (Immerzeel et al., 2019), which, combined with an increasing population, would lead to an even higher water stress. Convective precipitation systems in this region are therefore a highly important resource of freshwater. In our results, it was also evident that MPSs contribute significantly to the total MJJAS precipitation, especially south of the Himalayas (Fig. 14). Additionally, in areas of quite low annual mean MJJAS sum of precipitation (e.g. southwest of the TP) (Fig. 13), MPSs contribution to total MJJAS

precipitation could still be high (Fig. 14). Based on these results, MPSs seems to be much involved in the region's water cycle providing a significant amount of precipitation. We could, however, also see that the results varied depending on spatial resolution and downscaling techniques, e.g. less MPSs in a spectral nudging 9 km non-CP simulation (WRF_GU) than in a re-initialized 10 km RCM simulation with CP (HAR) (Table 1 & Fig. 12). Fully understanding this difference could bring further knowledge in how mesoscale processes are resolved in various RCM simulations. This could later be valuable information and possibly improve the accuracy in future projections of convective systems.

Convective systems can also be hazardous, bringing intense precipitation at a short period of time resulting in floods (Rasmussen & Houze, 2012). In a study by Rasmussen & Houze (2012), a disastrous flash-flood in the Himalayas was found to originate from MCSs formed on the TP. As these moved out from the plateau, moist air from the Arabian Sea and BoB enhanced the systems further which resulted in intense precipitation and flash-floods (Rasmussen & Houze, 2012). Another hazardous system is the TPV, which has also been shown to cause extreme rainfall events if moving off the plateau (Li et al., 2021). The need for understanding convective systems and mesoscale processes is therefore great, especially in mountainous regions since the effect can be hazardous. In our results, the global reanalysis dataset of coarse resolution (ERA5) did not detect any significant amount of MPSs over the TP, while both RCM simulations (WRF_GU and HAR) did (Table 1). As a result, information such as the most common hour of convection over the TP (Fig. 5), and location of initiation (Fig. 12), could be provided. This might argue for the benefits of using RCM simulations and the need in their ability to accurately project convective processes and systems at the mesoscale. However, since the satellite observations used as reference data did not detect any MPSs over the TP, the accuracy of the RCM simulations cannot be determined. Further analyses with various reference data would therefore be needed, but much interesting, for a conclusion. Still, the results of WRF_GU and HAR indicates that RCM simulation are able to detect convective systems in a complex region such as the TP.

Our results showed that MPSs are much involved in the hydrological cycle of the TP region. By producing information of the MPSs at every timestep of their lifecycle, we could e.g. see that they intensified over time and that their diurnal cycle was more pronounced at higher intensity levels (Fig. 6 & 10). This means that longer lived systems are more prone to produce intense precipitation. It also means that intense precipitation systems have more distinct peaks and lows during a day than smaller ones. Such information can be much valuable in further analyses of mesoscale convection using RCMs, as there is a need to improve their spatiotemporal accuracy in modelling these processes in mountainous regions (Yao et al., 2022).

4.6 Sources of uncertainties

4.6.1 Reference data

The GPM IMERGE Final Run (GPM) satellite product used for comparison in our report has been shown by previous studies to contain uncertainties in its precipitation estimates, both in regions consisting of complex topography (e.g. over the

Himalayan foothills (Prakash et al., 2018) and the mountainous regions of Iran (Sharifi et al., 2016)), but also in regions of more homogenous topography such as the Chindwin River basin in northwestern Myanmar (Yuan et al., 2017) and northeastern India (Prakash et al., 2018). Although we did find areas with higher amount of precipitation in WRF_GU, HAR and ERA5 compared to GPM (Fig. 13), the number of MPSs detected by the GPM dataset (Table 1) and their spatial distribution density (Fig. 12) were still relatively high and, in these statistics, WRF_GU was the one dataset with overall lowest values. We could also see that GPM and WRF_GU were the two datasets with strongest tendency to detect MPSs with a higher intensity level (Fig. 7). Similar issues have been discussed in an article by Xu et al., (2017), in which they focused on the southern TP and only on domains where rain gauge stations exists to enable a direct comparison. In their results, it was detected that light rain events ($0 – 1$ mm d^{-1}) were underestimated and misrepresented by GPM, while intense rainfall event frequency (>10 mm d^{-1}) was overestimated (Xu et al., 2017). The findings of Xu et al., (2017) might explain why the precipitation amount in our GPM results was, in some regions, lower than in remaining datasets and why the GPM dataset detected MPSs with a high intensity level. This also suggests that, although GPM might have underestimated precipitation, it was still able to detect MPSs as these had to fulfill a minimum of 3 mm h^{-1} criterion. Still, both the method and study area used by Xu et al., (2017) differed to our study and further research would therefore be needed to draw any major conclusion based on our results.

4.6.2 The WRF model

Although spectral nudging and re-initialization have been shown to be valid techniques in regional climate models for dynamical downscaling in representing convection, convergence and precipitation (Bowden et al., 2012; Bullock et al., 2014; Lo et al., 2008; Ma et al., 2022; Otte et al., 2012; Ou et al., 2020; Song et al., 2011), wet biases have been found when using the WRF model (Bullock et al., 2014; Otte et al., 2012). This was also evident in our mean MJJAS sum of precipitation results where both WRF_GU and HAR had areas of unusually high values (Fig. 13). To reduce this wet bias and improve the spectral nudging technique in WRF model simulations, Spero et al., (2014) applied nudging of moisture below the tropopause which resulted in a better representation of clouds, radiation and precipitation. This further highlights the complexity in dynamical downscaling and how various techniques and models can be useful but also cause errors. In this study, focus has been on MPSs as convective precipitation systems and although there was an indication for a wet bias in both WRF_GU and HAR, this seems to have played a less important role for our focus points since the MPS density results of WRF_GU and HAR ended up being restrained (WRF_GU) and excessive (HAR) to that of GPM (Fig. 12). In context to our research, GPM was, together with WRF_GU, the dataset with highest tendency to detect MPSs with more intense precipitation (Fig. 7). We can therefore not conclude if the WRF model has caused any errors per se.

4.6.3 Tobac algorithm

In the lifetime analysis of MPSs there were some outliers, especially in HAR and ERA5 in the extensive domain (Fig. 8), which could be due to the tobac algorithm used for tracking MPSs. In this case, however, we first need to explain the term feature. The tobac algorithm uses the term feature for a precipitation system at a certain step, fulfilling some but not all

thresholds (Heikenfeld et al., 2019). In our case, a feature could be translated into a precipitation system at step 1 (see sect 2.2.2), fulfilling size and intensity but not yet duration. So, in the tobac algorithm, there is an option where a feature can miss out on several timesteps of a precipitation system's lifecycle, but still get linked to that system on a later stage (Heikenfeld et al., 2019). According to Heikenfeld et al., (2019), however, this can lead to errors as clouds formed in the vicinity of a precipitation system could be identified as features of that system, rather than features of a newly formed independent one.

4.6.4 Temporal resolution

This problem will be of greater concern if you were to use an input dataset of low temporal resolution (Heikenfeld et al., 2019). As shown in an example by Heikenfeld et al., (2019), a temporal resolution lower than 15 minutes could result in an overlap between older and newly formed features. They argue that this is because the location and motion of the next feature of an existing precipitation system is predicted based on previous features propagation speed. So by using a lower temporal resolution, the possible area of the next feature will thereby increase significantly (Heikenfeld et al., 2019). A lower temporal resolution might, therefore, enable overlapping with other features which do not necessarily belong to the actual precipitation system but will be identified as such due to similar properties.

In our tracking, the WRF_GU, HAR and ERA5 datasets all have a temporal resolution of one hour, while GPM has 30 minutes and they are, according to Heikenfeld et al., (2019), all to be considered as a low temporal resolution dataset. This might therefore explain the outliers of max MPS lifetime found and why GPM had a more concentrated lifetime distribution compared to the remaining datasets, as it had the highest temporal resolution. In contrast to other climate model simulation and reanalysis datasets, however, a temporal resolution of one hour is still quite high. For example, both the predecessor to ERA5, ERA-Interim, and the NCEP/NCAR global reanalysis datasets have a temporal resolution of six hour (Hersbach et al., 2020; Kalnay et al., 1996).

4.6.5 Thresholds defining an MPS

Another reason for the lifetime analysis outliers could be that our results mainly consist of smaller systems with an overall lower lifetime, and that the outliers actually are larger systems. Previous studies have shown that convective precipitation systems at the 30°N latitude can last between 10 – 18h (Feng et al., 2021), in the tropical Pacific warm pool between 8 – 20h (Chen & Houze, 1997) and over the TP for as long as 36h (Yaodong et al., 2008), but also for 12h (Hu et al., 2016) and as short as 6h (Mai et al., 2021). Our observational dataset (GPM) used for comparison and the one with most concentrated distribution of lifetime resulted in an MPS duration between 4 – 6h, while the two datasets with highest number of outliers and highest duration of outlier's lifetime, HAR and ERA5, had the widest lifetime distribution results with an MPS duration between 4 – 9 and 4 – 10h respectively (Fig. 8). The location of a convective precipitation system is therefore an important aspect which might impact its lifetime, but also the definition and size threshold used in tracking the system of interest. As discussed by Mai et al., (2021), one of the reasons for their much lower average lifetime results was due to using a lower

threshold for their convective precipitation systems minimum size and that larger systems are usually coherent with longer lifetime overall. Although we also used a wider definition for an MPS with a lower minimum size threshold, our MPS lifetime results were still shorter than those of Mai et al., (2021) regarding the TP domain results, while in the vicinity in the larger extensive domain. They did, however, focus on MCSs including a temperature threshold in their tracking, while we rather focused on precipitation. Due to the distinct definitions and techniques used for tracking convective precipitation systems, the MPS lifetime durations of our results seem reasonable as we have included all convective precipitation systems larger than local and not only one type of convective precipitation system. Although future research with a higher temporal resolution dataset used for comparison, or one exploring the various definitions of a convective precipitation system and its impact on the size and lifetime results would be interesting, the intentions of this research project could be fulfilled.

4.7 Further research

We did not analyze the movements of the MPSs, so it is not known whether or not TP domain MPSs have been lasting their entire lifetime over the plateau, originating from it, or dissipating on it. But due to the diurnal cycle results (Fig. 5) and low number of MPSs in ERA5 (Table 1), we believe that most of the MPSs of WRF_GU, HAR and GPM originates on the plateau while ERA5 had MPSs moving in over the plateau from adjacent regions. A conclusion in the matter would, however, need a movement analysis and it would be interesting to incorporate one in future research. A movement analysis would also be useful to investigate the MPS contribution to total precipitation during its lifecycle, as it was detectable that areas of low MPS density could still have a high contribution to total precipitation, mainly in dry regions (Fig. 14). This was evident in the southwestern parts of the extensive domain in all datasets and north-northeast of the TP in WRF_GU and HAR. These results suggests that, in dry regions, one MPS is enough to contribute with the majority of that areas mean MJJAS sum of precipitation. Further, by including the intensity level of an MPS during its lifecycle in a movement analysis, it could also bring further knowledge to the discussion of what impacts a higher intensity level, as we then could investigate where and in what stage an MPS would have its highest intensity level.

5 Conclusions

What are the main characteristics of mesoscale precipitation systems (MPS) in the TP region between 2001 – 2016?

It was evident in our results that the regional climate and topography of the TP both played an important role in MPS formation and distribution. By analyzing the diurnal cycle of MPS convection, early morning peaks of convection were found in the extensive domain. These were most likely a result of the monsoonal southwesterly wind flows, as these bring moist air from the Bay of Bengal (BoB) and Arabian Sea and have been shown to trigger convection post-midnight. Since the highest density of MPSs found were located south of the TP where these wind flows are dominating, it could be concluded that they have a great impact on the timing and location of MPS formation in the TP region. Another factor concluded to be of importance was the topography of the TP, since it causes a nocturnal cooling of air which triggers convection south of the Himalayan mountain range. In the TP domain, due to its altitude, strong daytime solar heating enabled convection in the afternoon instead, coherent with previous findings adding further validity for this argument. It could also be concluded that an intensity level of an MPS was not related to the actual size of the MPS, but rather to its lifetime, lifecycle development and regional climatic patterns.

How do these differ in the three model/reanalysis datasets that represent different spatial resolution?

Based on the results, it could be concluded that the 31km grid spaced global reanalysis dataset of ERA5 was too coarse to detect convection at an early stage of an MPS. Another factor shown to impact the delay and larger MPSs in ERA5 was topographic features. Again, due to its coarse spatial resolution, ERA5 was not able to represent topographic features as well as a finer resolution dataset, resulting in a later detection of MPS formation. These results highlight the added value of using a finer resolution dataset such as WRF_GU (9km) or HAR (10km), when conducting convection analyses in mountainous regions.

It was also shown that convection parameterization (CP) could have caused excessive convection, since the datasets using CP in this report (HAR and ERA5) resulted in higher number and density of MPSs than the non-CP dataset (WRF_GU) and satellite observations (GPM). It could, however, not be concluded whether or not a non-CP simulation outperformed a CP model simulation, although implications were found. Further analyses in the gray-zone of climate modelling with and without CP is therefore needed for a conclusion in the matter.

Which of the two downscaling techniques (HAR and WRF_GU) result in the better representation of mesoscale precipitation systems compared to GPM satellite observations?

By using spectral nudging, the monsoonal southwesterly wind flows in the region impacting MPS formation have been shown to be better represented. It has also been shown that re-initialization can trigger excessive convergence and precipitation in these regions. Now, although HAR resulted in a higher MPS density than GPM, WRF_GU resulted in the opposite, and both did result in excessive precipitation compared to GPM. It could therefore not be concluded which of the two downscaling

techniques better represented MPSs in the TP region compared to GPM. What we could conclude, however, is that CP and re-initialization caused excessive convection while a non-CP simulation using spectral nudging resulted in the opposite.

References

Bao, Q., & Li, J. (2020). Progress in climate modeling of precipitation over the Tibetan Plateau. *National Science Review*, *7*(3), 486–487. https://doi.org/10.1093/nsr/nwaa006

Bowden, J. H., Otte, T. L., Nolte, C. G., & Otte, M. J. (2012). Examining interior grid nudging techniques using two-way nesting in the WRF model for regional climate modeling. *Journal of Climate*, *25*(8), 2805–2823. https://doi.org/10.1175/JCLI-D-11-00167.1

Bullock, O. R., Alapaty, K., Herwehe, J. A., Mallard, M. S., Otte, T. L., Gilliam, R. C., & Nolte, C. G. (2014). An observation-based investigation of nudging in WRF for downscaling surface climate information to 12-km grid spacing. *Journal of Applied Meteorology and Climatology*, *53*(1), 20–33. https://doi.org/10.1175/JAMC-D-13-030.1

Chen, S. S., & Houze, R. A. (1997). Diurnal variation and life-cycle of deep convective systems over the tropical Pacific warm pool. *Quarterly Journal of the Royal Meteorological Society*, *123*(538), 357–388. https://doi.org/10.1256/smsqj.53805

Clark, P., Roberts, N., Lean, H., Ballard, S. P., & Charlton-Perez, C. (2016). Convection-permitting models: A step-change in rainfall forecasting. *Meteorological Applications*, *23*(2), 165–181. https://doi.org/10.1002/met.1538

Crook, N. A., & Moncrieff, M. W. (1988). The effect of large-scale convergence on the generation and maintenance of deep moist convection. *Journal of the Atmospheric Sciences*, *45*(23), 3606–3624.

Curio, J., & Scherer, D. (2016). Seasonality and spatial variability of dynamic precipitation controls on the Tibetan Plateau. *Earth System Dynamics*, *7*(3), 767–782. https://doi.org/10.5194/esd-7-767-2016

Curio, J., Schiemannm, R., Hodges, K. I., & Turner, A. G. (2019). Climatology of Tibetan Plateau vortices in reanalysis data and a high-resolution global climate model. *Journal of Climate*, *32*(6), 1933–1950.

Davis, C. A., Brown, B., & Bullock, R. (2006). Object-based verification of precipitation forecasts. Part I: Application to convective rain systems. *Monthly Weather Review*, *134*(7), 1785–1795. https://doi.org/10.1175/MWR3146.1

Davis, C., Brown, B., & Bullock, R. (2006). Object-based verification of precipitation forecasts. Part II: Application to convective rain systems. *Monthly Weather Review*, *134*(7), 1785–1795.

Doswell III, C. A. (1987). The distinction between large-scale and mesoscale contribution to severe convection: A case study example. *Weather and Forecasting*, *2*(1), 3–16.

Ebert, E. E., & McBride, J. L. (2000). Verification of precipitation in weather systems: Determination of systematic errors. *Journal of Hydrology*, *239*(1–4), 179–202.

Feng, X., Liu, C., Rasmussen, R., & Fan, G. (2014). A 10-yr climatology of tibetan plateau vortices with NCEP climate forecast system reanalysis. *Journal of Applied Meteorology and Climatology*, *53*(1), 34–46. https://doi.org/10.1175/JAMC-D-13-014.1

Feng, Z., Leung, L. R., Liu, N., Wang, J., Houze, R. A., Li, J., Hardin, J. C., Chen, D., & Guo, J. (2021). A Global High-Resolution Mesoscale Convective System Database Using Satellite-Derived Cloud Tops, Surface Precipitation, and Tracking. *Journal of Geophysical Research: Atmospheres*, *126*(8), 1–29. https://doi.org/10.1029/2020JD034202

Feser, F., Rockel, B., Von Storch, H., Winterfeldt, J., & Zahn, M. (2011). Regional Climate Models Add Value to Global Model Data: A Review and Selected Examples. *Bulletin of the American Meteorological Society*, *92*(9), 1181–1192. https://doi.org/10.1175/2011bams3061.1

Finney, D. L., Marsham, J. H., Jackson, L. S., Kendon, E. J., Rowell, D. P., Boorman, P. M., Keane, R. J., Stratton, R. A., & Senior, C. A. (2019). Implications of improved representation of convection for the East Africa water budget using a convection-permitting model. *Journal of Climate*, *32*(7), 2109–2129. https://doi.org/10.1175/JCLI-D-18-0387.1

Giorgi, F., & Mearns, L. O. (1999). Introduction to special section: Regional climate modeling revisited. *Journal of Geophysical Research: Atmospheres*, *104*(D6), 6335–6352. https://doi.org/10.1029/98JD02072

Heikenfeld, M., Marinescu, P. J., Christensen, M., Watson-Parris, D., Senf, F., Van Den Heever, S. C., & Stier, P. (2019). Tobac 1.2: Towards a flexible framework for tracking and analysis of clouds in diverse datasets. *Geoscientific Model Development*, *12*(11), 4551–4570. https://doi.org/10.5194/gmd-12-4551-2019

Hersbach, H., Bell, B., Berrisford, P., Hirahara, S., Horányi, A., Muñoz-Sabater, J., Nicolas, J., Peubey, C., Radu, R., Schepers, D., Simmons, A., Soci, C., Abdalla, S., Abellan, X., Balsamo, G., Bechtold, P., Biavati, G., Bidlot, J., Bonavita, M., … Thépaut, J. (2020). The ERA5 global reanalysis. *Quarterly Journal of the Royal Meteorological Society*, *146*(730), 1999–2049. https://doi.org/10.1002/qj.3803

Hou, A. Y., Kakar, R. K., Neeck, S., Azarbarzin, A. A., Kummerow, C. D., Kojima, M., Oki, R., Nakamura, K., & Iguchi, T. (2014). The Global Precipitation Measurement Mission. *Bulletin of the American Meteorological Society*, *95*(5), 701–722. https://doi.org/10.1175/bams-d-13-00164.1

Houze Jr, R. A. (1981). Structures of atmospheric precipitation systems: A global survey. *Radio Science*, *16*(5), 671–689.

Houze Jr, R. A. (2004). Mesoscale convective systems. *Reviews of Geophysics*, *42*(4).

Houze Jr, R. A., Wilton, D. C., & Smull, B. F. (2007). Monsoon convection in the Himalayan region as seen by the TRMM Precipitation Radar. *Quarterly Journal of the Royal Meteorological Society: A Journal of the Atmospheric Sciences, Applied Meteorology and Physical Oceanography*, *133*(627), 1389–1411.

Houze, R. A. (2012). Orographic effects on precipitating clouds. *Reviews of Geophysics*, *50*(1), 1–47. https://doi.org/10.1029/2011RG000365

Hu, L., Deng, D., Gao, S., & Xu, X. (2016). The seasonal variation of Tibetan convective systems: Satellite observation. *Journal of Geophysical Research: Atmospheres*, *121*(10), 5512–5525.

Hu, L., Deng, D., Xu, X., & Zhao, P. (2017). The regional differences of Tibetan convective systems in boreal summer. *Journal of Geophysical Research: Atmospheres*, *122*(14), 7289–7299. https://doi.org/10.1002/2017jd026681

Immerzeel, W W, Lutz, A. F., Andrade, M., Bahl, A., Biemans, H., Bolch, T., Hyde, S., Brumby, S., Davies, B. J., Elmore, A. C., Emmer, A., Feng, M., Fernández, A., Haritashya, U., Kargel, J. S., Koppes, M., Kraaijenbrink, P. D. A., Kulkarni, A. V, Mayewski, P. A., … Baillie, J. E. M. (2019). Importance and vulnerability of the world's water towers. *Nature*, *577*(7790), 364–369. https://doi.org/10.1038/s41586-019-1822-y

Immerzeel, Walter W, Van Beek, L. P. H., & Bierkens, M. F. P. (2010). Climate change will affect the Asian water towers.

Science, *328*(5984), 1382–1385.

Kalnay, E., Kanamitsu, M., Kistler, R., Collins, W., Deaven, D., & Gandin, L. (1996). *The NCEP / NCAR 40-Year Reanalysis Project*.

Kirshbaum, D. J. (2020). Numerical simulations of orographic convection across multiple gray zones. *Journal of the Atmospheric Sciences*, *77*(10), 3301–3320. https://doi.org/10.1175/JAS-D-20-0035.1

Kotal, S. D., Roy, S. Sen, & Roy Bhowmik, S. K. (2014). Catastrophic heavy rainfall episode over Uttarakhand during 16-18 June 2013 - observational aspects. *Current Science*, *107*(2), 234–245. https://doi.org/10.18520/cs/v107/i2/234-245

Kukulies, J., Chen, D., & Curio, J. (2021). The Role of Mesoscale Convective Systems in Precipitation in the Tibetan Plateau Region. *Journal of Geophysical Research: Atmospheres*, *126*(23). https://doi.org/10.1029/2021jd035279

Kuo, Y.-H., Cheng, L., & Anthes, R. A. (1986). Mesoscale analyses of the Sichuan flood catastrophe, 11–15 July 1981. *Monthly Weather Review*, *114*(11), 1984–2003.

Li, L., Zhu, C., Zhang, R., & Liu, B. (2021). Roles of the Tibetan Plateau vortices in the record Meiyu rainfall in 2020. *Atmospheric Science Letters*, *22*(3), 1–9. https://doi.org/10.1002/asl.1017

Lin, C., Chen, D., Yang, K., & Ou, T. (2018). Impact of model resolution on simulating the water vapor transport through the central Himalayas: implication for models' wet bias over the Tibetan Plateau. *Climate Dynamics*, *51*(9–10), 3195–3207. https://doi.org/10.1007/s00382-018-4074-x

Liu, L., Zheng, J., Ruan, Z., Cui, Z., Hu, Z., Wu, S., Dai, G., & Wu, Y. (2015). Comprehensive radar observations of clouds and precipitation over the tibetan plateau and preliminary analysis of cloud properties. *Journal of Meteorological Research*, *29*(4), 546–561. https://doi.org/10.1007/s13351-015-4208-6

Lo, J. C.-F., Yang, Z.-L., & Pielke, R. A. (2008). Assessment of three dynamical climate downscaling methods using the Weather Research and Forecasting (WRF) model. *Journal of Geophysical Research*, *113*(D9). https://doi.org/10.1029/2007jd009216

Ma, M., Hui, P., Liu, D., Zhou, P., & Tang, J. (2022). Convection-permitting regional climate simulations over Tibetan Plateau: re-initialization versus spectral nudging. *Climate Dynamics*, *58*(5–6), 1719–1735. https://doi.org/10.1007/s00382-021-05988-2

Mai, Z., Fu, S., Sun, J., Hu, L., & Wang, X. (2021). Key statistical characteristics of the mesoscale convective systems generated over the Tibetan Plateau and their relationship to precipitation and southwest vortices. *International Journal of Climatology*, *41*, E875–E896.

Maussion, F., Scherer, D., Mölg, T., Collier, E., Curio, J., & Finkelnburg, R. (2014). Precipitation Seasonality and Variability over the Tibetan Plateau as Resolved by the High Asia Reanalysis*. *Journal of Climate*, *27*(5), 1910–1927. https://doi.org/10.1175/jcli-d-13-00282.1

Medina, S., Houze, R. A., Kumar, A., & Niyogi, D. (2010). Summer monsoon convection in the Himalayan region: Terrain and land cover effects. *Quarterly Journal of the Royal Meteorological Society*, *136*(648), 593–616. https://doi.org/10.1002/qj.601

Orlanski, I. (1975). A rational subdivision of scales for atmospheric processes. *Bulletin of the American Meteorological Society*, 527–530.

Otte, T. L., Nolte, C. G., Otte, M. J., & Bowden, J. H. (2012). Does nudging squelch the extremes in regional climate modeling? *Journal of Climate*, *25*(20), 7046–7066. https://doi.org/10.1175/JCLI-D-12-00048.1

Ou, T., Chen, D., Chen, X., Lin, C., Yang, K., Lai, H.-W., & Zhang, F. (2020). Simulation of summer precipitation diurnal cycles over the Tibetan Plateau at the gray-zone grid spacing for cumulus parameterization. *Climate Dynamics*, *54*(7–8), 3525–3539. https://doi.org/10.1007/s00382-020-05181-x

Pan, Z., Takle, E., Gutowski, W., & Turner, R. (1999). Long simulation of regional climate as a sequence of short segments. *Monthly Weather Review*, *127*(2–3), 308–321. https://doi.org/10.1175/1520-0493(1999)127<0308:lsorca>2.0.co;2

Pearson, K. J., Lister, G. M. S., Birch, C. E., Allan, R. P., Hogan, R. J., & Woolnough, S. J. (2014). Modelling the diurnal cycle of tropical convection across the "grey zone." *Quarterly Journal of the Royal Meteorological Society*, *140*(679), 491–499. https://doi.org/10.1002/qj.2145

Prakash, S., Mitra, A. K., AghaKouchak, A., Liu, Z., Norouzi, H., & Pai, D. S. (2018). A preliminary assessment of GPM-based multi-satellite precipitation estimates over a monsoon dominated region. *Journal of Hydrology*, *556*(February 2014), 865–876. https://doi.org/10.1016/j.jhydrol.2016.01.029

Prein, A. F., Gobiet, A., Suklitsch, M., Truhetz, H., Awan, N. K., Keuler, K., & Georgievski, G. (2013). Added value of convection permitting seasonal simulations. *Climate Dynamics*, *41*(9–10), 2655–2677. https://doi.org/10.1007/s00382-013-1744-6

Prein, A. F., Rasmussen, R. M., Wang, D., & Giangrande, S. E. (2021). Sensitivity of organized convective storms to model grid spacing in current and future climates. *Philosophical Transactions of the Royal Society A: Mathematical, Physical and Engineering Sciences*, *379*(2195). https://doi.org/10.1098/rsta.2019.0546

Prein, Andreas F., Langhans, W., Fosser, G., Ferrone, A., Ban, N., Goergen, K., Keller, M., Tölle, M., Gutjahr, O., Feser, F., Brisson, E., Kollet, S., Schmidli, J., Van Lipzig, N. P. M., & Leung, R. (2015). A review on regional convection-permitting climate modeling: Demonstrations, prospects, and challenges. *Reviews of Geophysics*, *53*(2), 323–361. https://doi.org/10.1002/2014RG000475

Qian, J. H., Seth, A., & Zebiak, S. (2003). Reinitialized versus continuous simulations for regional climate downscaling. *Monthly Weather Review*, *131*(11), 2857–2874. https://doi.org/10.1175/1520-0493(2003)131<2857:RVCSFR>2.0.CO;2

Qin, J., Yang, K., Liang, S., & Guo, X. (2009). The altitudinal dependence of recent rapid warming over the Tibetan Plateau. *Climatic Change*, *97*(1–2), 321–327. https://doi.org/10.1007/s10584-009-9733-9

Qiu, J. (2008). China: the third pole. *Nature News*, *454*(7203), 393–396.

Rasmussen, K. L., & Houze, R. A. (2012). A Flash-Flooding Storm at the Steep Edge of High Terrain: Disaster in the Himalayas. *Bulletin of the American Meteorological Society*, *93*(11), 1713–1724. https://doi.org/10.1175/bams-d-11-00236.1

Romatschke, U., & Houze, R. A. (2011). Characteristics of precipitating convective systems in the South Asian monsoon. *Journal of Hydrometeorology*, *12*(1), 3–26. https://doi.org/10.1175/2010JHM1289.1

Rummukainen, M. (2010). State-of-the-art with regional. *Clim Change*, *1*(1), 82–96. https://doi.org/10.1002/wcc.008

Sato, T., & Kimura, F. (2007). How does the Tibetan Plateau affect the transition of Indian monsoon rainfall? *Monthly Weather Review*, *135*(5), 2006–2015. https://doi.org/10.1175/MWR3386.1

Sato, T., Yoshikane, T., Satoh, M., Miura, H., & Fujinami, H. (2008). Resolution Dependency of the Diurnal Cycle of Convective Clouds over the Tibetan Plateau in a Mesoscale Model. *Journal of the Meteorological Society of Japan. Ser. II*, *86A*, 17–31. https://doi.org/10.2151/jmsj.86a.17

Scaff, L., Prein, A. F., Li, Y., Liu, C., Rasmussen, R., & Ikeda, K. (2020). Simulating the convective precipitation diurnal cycle in North America's current and future climate. *Climate Dynamics*, *55*(1–2), 369–382. https://doi.org/10.1007/s00382-019-04754-9

Schumacher, R. S., & Johnson, R. H. (2005). Organization and environmental properties of extreme-rain-producing mesoscale convective systems. *Monthly Weather Review*, *133*(4), 961–976. https://doi.org/10.1175/MWR2899.1

Schumacher, R. S., & Rasmussen, K. L. (2020). The formation, character and changing nature of mesoscale convective systems. *Nature Reviews Earth and Environment*, *1*(6), 300–314. https://doi.org/10.1038/s43017-020-0057-7

Sharifi, E., Steinacker, R., & Saghafian, B. (2016). Assessment of GPM-IMERG and other precipitation products against gauge data under different topographic and climatic conditions in Iran: Preliminary results. *Remote Sensing*, *8*(2). https://doi.org/10.3390/rs8020135

Shepherd, T. G. (2014). Atmospheric circulation as a source of uncertainty in climate change projections. *Nature Geoscience*, *7*(10), 703–708. https://doi.org/10.1038/NGEO2253

Song, S., Tang, J., & Chen, X. (2011). Impacts of spectral nudging on the sensitivity of a regional climate model to convective parameterizations in East Asia. *Acta Meteorologica Sinica*, *25*(1), 63–77. https://doi.org/10.1007/s13351-011-0005-z

Spero, T. L., Otte, M. J., Bowden, J. H., & Nolte, C. G. (2014). Journal of geophysical research. *Nature*, *175*(4449), 238. https://doi.org/10.1038/175238c0

Sugimoto, S., & Ueno, K. (2012). Role of Mesoscale Convective Systems Developed around the Eastern Tibetan Plateau in the Eastward Expansion of an Upper Tropospheric High during the Monsoon Season. *Journal of the Meteorological Society of Japan. Ser. II*, *90*(2), 297–310. https://doi.org/10.2151/jmsj.2012-209

Von Storch, H., Langenberg, H., & Feser, F. (2000). A Spectral Nudging Technique for Dynamical Downscaling Purposes. *Monthly Weather Review*, *128*(10), 3664–3673. https://doi.org/10.1175/1520-0493(2000)128<3664:asntfd>2.0.co;2

Wagner, A., Heinzeller, D., Wagner, S., Rummler, T., & Kunstmann, H. (2018). Explicit convection and scale-aware cumulus parameterizations: High-resolution simulations over areas of different topography in Germany. *Monthly Weather Review*, *146*(6), 1925–1944. https://doi.org/10.1175/MWR-D-17-0238.1

Waldron, K. M., Paegle, J., & Horel, J. D. (1996). Sensitivity of a spectrally filtered and nudged limited-area model to outer model options. *Monthly Weather Review*, *124*(3), 529–547.

Wang, Xuejia, Pang, G., & Yang, M. (2018). Precipitation over the tibetan plateau during recent decades: A review based on observations and simulations. *International Journal of Climatology*, *38*(3), 1116–1131. https://doi.org/10.1002/joc.5246

Wang, Xun, Tolksdorf, V., Otto, M., & Scherer, D. (2021). WRF-based dynamical downscaling of ERA5 reanalysis data for High Mountain Asia: Towards a new version of the High Asia Refined analysis. *International Journal of Climatology*, *41*(1), 743–762. https://doi.org/10.1002/joc.6686

Weisman, M. L., Skamarock, W. C., & Klemp, J. B. (1997). The Resolution Dependence of Explicitly Modeled Convective Systems. *Monthly Weather Review*, *125*(4), 527–548. https://doi.org/10.1175/1520-0493(1997)125<0527:trdoem>2.0.co;2

Xu, R., Tian, F., Yang, L., Hu, H., Lu, H., & Hou, A. (2017). Ground validation of GPM IMERG and trmm 3B42V7 rainfall products over Southern Tibetan plateau based on a high-density rain gauge network. *Journal of Geophysical Research*, *122*(2), 910–924. https://doi.org/10.1002/2016JD025418

Yanai, M., & Wu, G.-X. (2006). Effects of the Tibetan plateau. In *The Asian Monsoon* (pp. 513–549). Springer.

Yao, T., Bolch, T., Chen, D., Gao, J., Immerzeel, W., Piao, S., Su, F., Thompson, L., Wada, Y., & Wang, L. (2022). The imbalance of the Asian water tower. *Nature Reviews Earth & Environment*, 1–15.

Yao, T., Liu, Y., Zhao, H., & Yu, W. (2011). *Tibetan Plateau* (pp. 1172–1175). Springer Netherlands. https://doi.org/10.1007/978-90-481-2642-2_578

Yaodong, L., Yun, W., Yang, S., Liang, H., Shouting, G., & Fu, R. (2008). Characteristics of Summer Convective Systems Initiated over the Tibetan Plateau. Part I: Origin, Track, Development, and Precipitation. *Journal of Applied Meteorology and Climatology*, *47*(10), 2679–2695. https://doi.org/10.1175/2008jamc1695.1

Ye, D. Z., & Wu, G. X. (1998). The role of the heat source of the Tibetan Plateau in the general circulation. *Meteorology and Atmospheric Physics*, *67*(1–4), 181–198. https://doi.org/10.1007/BF01277509

Ye, H., Fetzer, E. J., Wong, S., & Lambrigtsen, B. H. (2017). Rapid decadal convective precipitation increase over Eurasia during the last three decades of the 20th century. *Science Advances*, *3*(1), e1600944.

Yu, X., & Lee, T. Y. (2010). Role of convective parameterization in simulations of a convection band at grey-zone resolutions. *Tellus, Series A: Dynamic Meteorology and Oceanography*, *62*(5), 617–632. https://doi.org/10.1111/j.1600-0870.2010.00470.x

Yuan, F., Zhang, L., Wah Win, K. W., Ren, L., Zhao, C., Zhu, Y., Jiang, S., & Liu, Y. (2017). Assessment of GPM and TRMM multi-satellite precipitation products in streamflow simulations in a data sparse mountainous watershed in Myanmar. *Remote Sensing*, *9*(3). https://doi.org/10.3390/rs9030302

Zhao, Y., Zhou, T., Li, P., Furtado, K., & Zou, L. (2021). Added Value of a Convection Permitting Model in Simulating Atmospheric Water Cycle Over the Asian Water Tower. *Journal of Geophysical Research: Atmospheres*, *126*(13), 1–17. https://doi.org/10.1029/2021JD034788